NASA Contractor Report 3433

Multiple-Scale Turbulence Modeling of Boundary Layer Flows for Scramjet Applications

G. Fabris, P. T. Harsha,
and R. B. Edelman

CONTRACT NAS1-15988
MAY 1981

NASA

NASA Contractor Report 3433

Multiple-Scale Turbulence Modeling of Boundary Layer Flows for Scramjet Applications

G. Fabris, P. T. Harsha,
and R. B. Edelman
Science Applications, Inc.
Canoga Park, California

Prepared for
Langley Research Center
under Contract NAS1-15988

National Aeronautics
and Space Administration

Scientific and Technical
Information Branch

1981

CONTENTS

LIST OF FIGURES

1. INTRODUCTION

The flowfields involved in advanced scramjet combustion systems are highly complex, three-dimensional supersonic flows with embedded subsonic regions and regions of recirculating flow. Problems of fuel injection and the finite-rate reaction chemistry of hydrogen and hydrocarbon fuels must also be considered. The critical interrelationship of all of the processes involved in a scramjet combustion system requires the development of analytical design tools to investigate in detail the combustor flowfield and provide design and scaling information. While considerable progress has been made in the development of analytic design tools (Ref. 1), the complexity of the problem requires further progress in a variety of areas.

A necessary feature of an advanced scramjet combustor model is the incorporation of a turbulence model that adequately accounts for the effects on the turbulent shear stress of the non-isotropy of elliptic flows, the effects of compressibility on turbulence, and the interaction between turbulence and the chemical reactions occurring within the flowfield. The turbulence model must be well-supported by experimental data, and sufficiently practical that its use does not require excessive computational time. It must also be reliable: sufficiently general that it can be applied with confidence to a variety of flows, and amenable to the use of estimated initial conditions when detailed initial turbulence data do not exist. However, since it can be expected that different effects may dominate in different regions of the flow: non-isotropy in recirculation regions; compressibility effects (including the effects of shock waves on turbulence structure) in high-speed flow regions; and turbulence-chemistry interaction effects in regions in which fuel ignition and combustion are occurring, a modular approach may be the most efficient overall. In such an approach, both the numerical solution procedure and the turbulence model are specialized to account for the particular phenomena that dominate a particular region of the flowfield.

There is a substantial variety of turbulence models that have been proposed for turbulent flows of interest in a scramjet combustor environment. These models range from algebraic eddy viscosity formulations, through one- and two-equation turbulent kinetic energy models, to multiple-equation Reynolds stress formulations and direct numerical turbulence simulations. The application of these models to a variety of turbulent flows, most of which are relevant to scramjet combustors, has been reviewed in detail by Schetz (Ref. 2). This review shows clearly that of all the turbulence models that have been developed, only the one- and two-equation turbulent kinetic energy approaches have been applied to a sufficient variety of flows to be considered reliable in scramjet applications. Eddy viscosity formulations do not provide the modeling of the evolution of turbulence structure that is required for a reliable and general model of the different phenomena which occur in a scramjet combustor, while Reynolds stress models and numerical turbulence simulations are far too complex and too little understood to be useful in engineering computations of combustor flowfields. Thus, the selection of models for scramjet combustor calculations can be narrowed immediately to the one- and two-equation turbulent kinetic energy approaches and the algebraic Reynolds stress formulation: the latter approach, which is not discussed by Schetz (Ref. 2), offers the potential of incorporating the turbulence viscosity non-isotropy aspects of a Reynolds stress formulation in an engineering model without the computational complexity inherent in the full Reynolds stress model.

Neither of the two turbulent kinetic energy approaches discussed by Schetz (Ref. 2) are directly usable as turbulence models for scramjet combustor applications. The one-equation formulation, which has been developed to include empirical adjustments for compressibility effects, requires the a priori specification of a turbulence length scale, and this scale cannot be satisfactorily specified in a complex flow. The two-equation model requires different coefficients for planar and axisymmetric flows and also requires empirical adjustments for compressibility effects. Neither of these models is capable of predicting the response of a turbulent flow to rapid pressure variations.

Recently, Launder and co-workers have initiated the development of a modified form of the two-equation approach which overcomes several of the problems encountered with this model (Refs. 3, 4, 5). The basic two-equation turbulence

model involves the solution of transport equations for the turbulent kinetic energy and its dissipation rate. This latter equation can be viewed as an equation for the distribution of turbulence length scale, which in turn can be interpreted as a measure of the average size of the eddies which make up a turbulent flow. A difficulty with this approach is that there is a vast size disparity between those eddies in which turbulence production takes place and the small eddies in which turbulence dissipation occurs. The description of the structure of a turbulent flow using a single average length scale implies that there is a constant relationship between the turbulence-production eddy scale and the turbulence-dissipation eddy scale and between turbulence-production and turbulence-dissipation rates. For some flows these rates do not maintain a constant proportionality and it is in these flows that the basic two-equation model fails. To overcome this problem, Launder and co-workers suggested a multiple-scale formulation.

The multiple-scale formulation is attractive for scramjet applications for several reasons. The most obvious attraction of the model is its potential to overcome the limitations on generality observed in applications of the basic two-equation model to axisymmetric and planar flows. Further, Launder and co-workers have shown (Ref. 5) that the multiple-scale formulation successfully predicts the development of the turbulence structure under rapid pressure variation, where the basic two-equation model also fails. But there are other potential areas in which the multiple-scale formulation has considerable merit, of which the most interesting is the problem of turbulence-chemistry interaction.

The attraction of the multiple-scale formulation in problems of turbulence-chemistry interaction lies in its ability to predict the coupled evolution of disparate length scales in a turbulent flow. It has long been recognized that the phenomenon of unmixedness in a turbulent flow is related to the evolution of small-scale eddies, and thus to the turbulence dissipation rate. On the other hand, the large-scale turbulent mixing process is related to the effective turbulent viscosity. Both the turbulence dissipation rate and the turbulent viscosity can be related to a turbulence length scale, but in inverse ways: the dissipation rate proportional to $k^{3/2}/\ell$ and the viscosity proportional to $k^{1/2}\ell$. Thus with a single-scale model, increases in length scale

which increase the turbulent mixing rate also imply a decreased dissipation rate and thus larger unmixedness effects. With a multiple-scale model, the effective viscosity length scale and the dissipation length scale are separately computed, so that unmixedness phenomena can, at least potentially, be more realistically examined and related to the rate of heat release.

The objective of this program is to develop accurate and reliable turbulence models suitable for use in predicting scramjet combustor flowfields. While it is recognized that because of the complexity of scramjet combustor flowfields, different models may be required for different parts of the flow, the potential for increased generality inherent in recent developments in turbulence modeling should be exploited. The multiple-scale formulation has been shown (Ref. 5) to overcome two of the major problems encountered in the use of the two-equation model, and thus it appears to be attractive for scramjet applications. However, it has not been used in a wide variety of flowfield predictions, so that its reliability is undetermined. Further, its use introduces at least two additional variables and transport equations, for which initial conditions must be provided, and the sensitivity of the model to initial condition specification is undocumented. Thus, an extensive investigation was carried out under this program to examine the capability of the multiple-scale formulation over as wide a variety of flows as possible, and to develop methods for the reliable estimation of the initial conditions required by the model. Because the bulk of the available data for model verification involves boundary layer type flows (jets, wakes, shear layers), most of the comparisons of model predictions with experimental data described in this report involve these flows. However, jets, wakes, and shear layers are fundamental parts of the complex flowfields encountered in scramjet combustion chambers; moreover, reliable numerical solution procedures exist for them, avoiding the problems of numerical solution inaccuracy which can complicate the interpretation of turbulence model performance in more complex flows.

In addition to the investigation of the multiple-scale model and initial condition estimation techniques, a number of other aspects of the problem of turbulence modeling for scramjet combustor applications have been considered in this program. Compressibility corrections to the dissipation equation have been evaluated in the context of the multiple-scale model. Recirculating

flowfields require the solution of the elliptic Navier-Stokes equations, and numerical solutions of these equations which are adequate for mean flowfield prediction are not, in general, adequate for turbulence model verification. Thus the application of elliptic solution techniques to recirculating flowfield prediction has been investigated to establish the grid resolution and convergence criteria required to adequately test different turbulence models. The algebraic Reynolds stress model defined by Rodi (Ref. 6) has been formulated for application to axisymmetric elliptic flows where shear non-isotropy effects may be important.

All of the work that has been carried out under this program to develop accurate and reliable turbulence models for scramjet combustor applications is described in detail in this report. The basic equations and turbulence model formulations are described in Section 2, which includes a description of the basic two-equation model, the algebraic Reynolds stress model, and the multiple-scale approach. Results of the application of the multiple-scale model to a variety of flowfields are described in Section 3, which includes a description of the results of the investigation of initial condition estimation techniques and of an initial investigation of compressibility corrections. The use of elliptic numerical techniques to provide solutions of recirculating flow problems suitable for the study of turbulence modeling is also discussed in this section. The results obtained from this program are discussed in Section 4, which also presents recommendations for further work in this area.

NOMENCLATURE

C	jet species concentrations
C_{p1}, C_{p2}, C'_{p1}, C_{T1}, C_{T2}, C_{μ}	multiple scale model coefficients defined by Eq. 22
D	jet diameter or planar body thickness
h'	enthalpy fluctuation
H	total enthalpy
k	turbulent kinetic energy
k_p	production-region turbulent kinetic energy, multiple-scale model
k_T	transfer-region turbulent kinetic energy, multiple-scale model
ℓ	turbulence dissipation rate length scale
m	turbulence-producing grid mesh size
M	Mach number
Ma	local Mach number
P	pressure
Pr	turbulent Prandtl number
Pr_k	turbulent Prandtl number for turbulent kinetic energy
r	radial coordinate

r_1 inlet radius

u_i i^{th} component of turbulent velocity fluctuation

U axial mean velocity component

U_i i^{th} component of mean velocity

V transverse or radial mean velocity component

x axial coordinate

x_i i^{th} component of Cartesian coordinate system

y lateral coordinate, planar flow

$y_{\frac{1}{2}}$ transverse distance at which $(U-U_I)/(U_I-U_E) = 0.5$ (shear layer)

$y_{0.1}$ transverse distance at which $(U-U_I)/(U_I-U_E) = 0.1$ (shear layer)

$y_{0.9}$ transverse distance at which $(U-U_I)/(U_I-U_E) = 0.9$ (shear layer)

Greek

α species mass fraction

δ_{ij} Kronecker delta, = 0 when $i \neq j$, = 1 when $i = j$

ε turbulent kinetic energy dissipation rate

ε_p turbulent kinetic energy dissipation rate, production region, multiple-scale model

ε_T turbulent kinetic energy dissipation rate, transfer region, multiple-scale model

κ wave number

μ dynamic viscosity

μ_{eff} turbulent effective dynamic viscosity

ν_T turbulent effective kinematic viscosity

ρ density

σ shear layer growth rate parameter

σ_0 shear layer growth rate parameter for $U_E/U_I = 0$

τ_{ij} shear stress tensor

ϕ generalized dependent variable

Subscripts

CL centerline value

E outer edge value

I inner edge value

j jet value

2. DESCRIPTION OF TURBULENCE MODELS

2.1 BASIC EQUATIONS: REYNOLDS AND FAVRE AVERAGING

Since direct solution of the time-dependent Navier-Stokes equations is practical for only a limited class of turbulent flows, the point of departure for practical problems involving turbulent flows are averaged versions of these equations. Averaged sets may be derived either through Reynolds (volume) averaging (Ref. 7) or Favre (mass) averaging (Ref. 8). In the Reynolds averaging procedure a given dependent variable, ϕ, is written in terms of its mean and fluctuating component,

$$\phi = \overline{\phi} + \phi'$$

where $\overline{\phi}' = 0$ and the overbar represents a time-average. In the case of Favre averaging, the basic relationship is

$$\bar{\rho}\phi = \overline{\rho\phi} + \bar{\rho}\phi'' = \bar{\rho}\tilde{\phi} + \bar{\rho}\phi''$$

or

$$\tilde{\phi} = \overline{\rho\phi}/\bar{\rho}$$

Under this definition

$$\overline{\phi}'' = (\bar{\rho}\tilde{\phi} - \overline{\rho\phi})/\bar{\rho} \neq 0$$

while

$$\overline{\rho\phi}'' = \overline{[\bar{\rho}(\rho\phi) - \rho(\overline{\rho\phi})]}/\bar{\rho} = 0$$

To compare the results of these two approaches, consider the momentum equation, which for a compressible flow is written, in Reynolds-average form

$$\bar{\rho}\frac{\partial \bar{U}_j}{\partial t} + (\bar{\rho}\bar{U}_i + \overline{\rho' u_i})\frac{\partial \bar{U}_j}{\partial x_i} = \frac{\partial}{\partial x_i}(\overline{\tau_{ij}} + \tau^T_{ij})$$

$$- \frac{\partial \bar{P}}{\partial x_i}\delta_{ij} - \overline{\rho' u_j}\frac{\partial \bar{U}_i}{\partial x_i} - \frac{\partial(\overline{\rho' u_j})}{\partial t} - \bar{U}_i\frac{\partial(\overline{\rho' u_j})}{\partial x_i} \qquad (1)$$

where

$$\tau_{ij} = \mu\left(\frac{\partial \bar{U}_j}{\partial x_i} + \frac{\partial \bar{U}_i}{\partial x_j}\right) - \frac{2}{3}\mu \frac{\partial \bar{U}_j}{\partial x_i} \delta_{ij}$$

and

$$\tau_{ij}^T = - \overline{\rho u_i u_i} - \overline{\rho' u_i u_j}$$

and in Favre-averaged form

$$\bar{\rho} \frac{\partial \hat{U}_j}{\partial t} + \bar{\rho} \hat{U}_j \frac{\partial \hat{U}_j}{\partial x_i} = - \frac{\partial P}{\partial x_j} \delta_{ij} + \frac{\partial}{\partial x_i} (\tau_{ij}^T + \tilde{\tau}_{ij} + \overline{\tau_{ij}''}) \qquad (2)$$

where

$$\tau_{ij}^T = - \overline{\rho' U_i'' U_j''}$$

$$\tilde{\tau}_{ij} = \mu\left[\frac{\partial \hat{U}_j}{\partial x_i} + \frac{\partial \hat{U}_i}{\partial x_j} - \frac{2}{3} \frac{\partial \hat{U}_j}{\partial x_i} \delta_{ij}\right]$$

and

$$\overline{\tau_{ij}''} = \mu\left[\overline{\frac{\partial u_j''}{\partial x_i} + \frac{\partial u_i''}{\partial x_i} - \frac{2}{3} \frac{\partial u_j''}{\partial x_i} \delta_{ij}}\right]$$

While at first glance the Favre-averaged equations appear to be considerably simpler than the Reynolds-averaged equations, closure hypotheses have in general been developed for the Reynolds-averaged equations. This situation exists for several reasons, of which the primary one is that most measurements of the correlations to date have been of the Reynolds-averaged correlations, in flows which are basically incompressible. Furthermore, Morkovin's hypothesis, that ρ' has a small effect on turbulence structure if $\rho'/\bar{\rho} \ll 1$, sanctions the use of incompressible turbulence models in a compressible flow for $M < 5$ in a boundary layer, $M < 1$ in a mixing layer, if mean density gradients have a small effect (Ref. 9).

In utilizing the Favre-averaged equations it is generally assumed that models developed for the Reynolds-averaged turbulence correlation terms are

also suitable for their Favre-averaged counterparts. This is often justified by observing that modeling the mass-averaged correlations in a manner similar to that in which the Reynolds-averaged correlations are modeled is preferable to the tacit neglect of the density fluctuation terms involved in modeling compressible flows using turbulence model equations derived from the incompressible Navier-Stokes equations (Ref. 8). It might also be noted that considerably fewer separate modeling assumptions are necessary when using the Favre-averaged equations relative to the Reynolds-averaged form, because of the grouping of terms inherent in Favre-averaging, although this advantage is considerably reduced by the inability to use available experimental data in carrying out the modeling.

If the modeling of the Favre-averaged equations is carried out along the lines outlined above, and the resulting equations are compared to the Reynolds equations, the comparison shows that the two sets of equations are equivalent as $\bar{u}_i \to \tilde{u}_i$. While this is not a surprising conclusion, as the limit $\bar{u}_i \to \tilde{u}_i$ implies $\rho'/\bar{\rho} \to 0$, the data of Stanford and Libby (Ref. 10) for a helium jet exhausting into air at low velocity shows that for this flow, the limit is nearly reached, i.e., $\bar{u}_i/\tilde{u}_i \simeq 1$. Although these data are for a relatively simple configuration, and extrapolation to flows with significant compressibility effects must be approached with caution, the helium-air system does involve a relatively large density ratio. Thus, in the context of utilizing the same modeling for the Favre-averaged equations as is used for the Reynolds-averaged equations, little is gained with respect to the turbulence modeling problem through use of the Favre-averaged form, and the Reynolds-averaged equations will be assumed in subsequent discussions.

2.2 CLOSURE HYPOTHESES FOR THE REYNOLDS-AVERAGED EQUATIONS - BOUNDARY LAYER FLOW

If Morkovin's hypothesis is invoked, so that terms involving density and pressure fluctuations can be neglected, and the molecular transport terms are neglected compared to the turbulent transport terms, the governing equations reduce, for steady flow of a single component gas to:

Continuity

$$\frac{\partial(\rho U_i)}{\partial x_i} = 0 \tag{3}$$

Momentum

$$\rho U_i \frac{\partial U_j}{\partial x_i} = - \frac{\partial}{\partial x_i} (\rho \overline{u_i u_j}) - \frac{\partial P}{\partial x_i} \delta_{ij} \tag{4}$$

Energy

$$\rho U_i \frac{\partial H}{\partial x_i} = - \frac{\partial}{\partial x_i} \left[\rho (\overline{u_i h' + u_i k}) \right] - \frac{\partial}{\partial x_i} (U_i \rho \overline{u_i u_j}) \tag{5}$$

where, in these equations, the overbars have been omitted from the mean parts of the dependent variables. Thus, closure hypotheses for this reduced set of equations reduce to obtaining expressions for the correlations $\rho\overline{u_i u_j}$, $\rho\overline{u_i h'}$, and $\rho\overline{u_i k}$. By far the most generally accepted approach to the required closure modeling for these equations is that involving the definition of an effective viscosity, i.e.,

$$-\rho\overline{u_i u_j} = \mu_{eff} \left(\frac{\partial U_j}{\partial x_i} + \frac{\partial U_i}{\partial x_j} \right) - \frac{2}{3} \rho k \delta_{ij} \tag{6}$$

$$-\rho\overline{u_i h'} = \frac{\mu_{eff}}{Pr} \left(\frac{\partial H}{\partial x_i} \right) \tag{7}$$

$$-\rho\overline{u_i k} = \frac{\mu_{eff}}{Pr_k} \left(\frac{\partial k}{\partial x_i} \right) \tag{8}$$

so that the additional closure assumption required involves a model for μ_{eff}. In Eqs. 6-8, Pr is the Prandtl number and Pr_k represents a Prandtl number for turbulent kinetic energy, $k = \frac{1}{2} \overline{u_i u_i}$. The most widely used model for μ_{eff} is the two-equation model, described by Launder, et al. (Ref. 11) and Launder and Spalding (Ref. 12); in this model

$$\mu_{eff} = C_\mu \rho k^2 / \varepsilon$$

where ε represents the turbulent kinetic energy dissipation rate and C_μ is a constant. The variables k and ε are themselves obtained from modeled transport equations derived from the (incompressible) Navier-Stokes equations, so that the two-equation model requires, in addition to Eqs. 6-8, the solution of:

Turbulent Kinetic Energy Transport

$$\frac{\partial}{\partial x_i}(\rho U_i k) = \frac{\partial}{\partial x_i}\left(\frac{\mu_{eff}}{Pr_k}\frac{\partial k}{\partial x_i}\right) - \rho\overline{u_i u_j}\frac{\partial U_i}{\partial x_j} - \rho\varepsilon \tag{9}$$

and

Turbulent Kinetic Energy Dissipation

$$\frac{\partial}{\partial x_i}(\rho U_i \varepsilon) = \frac{\partial}{\partial x_i}\left(\frac{\mu_{eff}}{Pr_\varepsilon}\frac{\partial \varepsilon}{\partial x_i}\right) - \frac{\varepsilon}{k}\left[C_{\varepsilon 1}\,\rho\overline{u_i u_j}\frac{\partial U_i}{\partial x_j} + C_{\varepsilon 2}\,\rho\varepsilon\right] \tag{10}$$

in which $C_{\varepsilon 1}$, $C_{\varepsilon 2}$, and Pr_ε are constants.

2.3 CLOSURE HYPOTHESES FOR THE REYNOLDS-AVERAGED EQUATIONS - ELLIPTIC FLOWS

The two-equation model has provided good results in boundary layer-type flows and some recirculating flows, and the multiple-scale formulation described in the next section offers promise of increasing the generality of the basic two-equation model. However, both of these models involve an isotropic viscosity assumption: that is, it is assumed in the formulation that the anisotropy of the Reynolds stresses is determined locally and that the principal axes of stress and strain are coincident. In some flows, this assumption may not be appropriate. An alternative to these approaches which does not involve an isotropic viscosity hypothesis is provided by Reynolds stress modeling, in which transport equations are solved for each of the $\overline{u_i u_j}$ components; the kinetic energy equation is obtained from the Reynolds stress equations when $i = j$. There are a number of postulated closures for the Reynolds stress equations, but Pope and Whitelaw (Ref. 13) note that these closures differ only in the term which represents redistribution of energy among the stress components (i.e., the tendency-toward-isotropy term).

In Ref. 13, Pope and Whitelaw carried out an assessment of two Reynolds stress models and the two-equation model, comparing detailed predictions of

mean flow and turbulence quantities with measurements obtained in planar and axisymmetric two-dimensional isothermal wakes. The conclusions of this study are of considerable interest here: in terms of mean velocity, little difference was observed between the predictions of the three models in the planar wake case, while for axisymmetric wakes the differences between the models were more strongly a function of the boundary conditions assumed than of the particular model used. That is, a change in assumptions regarding the boundary conditions produces a greater change in the predictions of all three turbulence models than the differences between the models for a given boundary condition.

For the axisymmetric wake with recirculation all of the models underpredict the length of the wake region and the rate of spread of the downstream wake. This deficiency is attributed by Pope and Whitelaw to the dissipation equation, which is common to both of the Reynolds stress models. It is of interest to note that both the modeling introduced by Launder for the solution of the planar-round jet discrepancy observed in the use of the two-equation model (Ref. 14) and the empirical compressibility corrections that have been applied to the one-equation turbulence model (Ref. 15) also involve the dissipation equation. Taken together, these observations suggest that improvements in dissipation equation modeling, which is a key element of the multiple-scale formulation, are necessary to provide increased generality of turbulence models.

Although Pope and Whitelaw (Ref. 13) note that through careful choice of a solution algorithm, it is possible to solve the five-equation Reynolds stress model with only 50% more computer time than the two-equation model; this increase in solution time could be significant in complex problems. An alternative approach, which still retains some of the ability of complete Reynolds stress models to predict non-isotropic flows, is the algebraic stress model proposed by Rodi (Ref. 6). Starting with the Reynolds stress equation, Rodi notes that if a consistent "simulation" of the convection and diffusion terms in this equation can be devised in terms of already computed quantities, then it reduces to an algebraic equation.

Although the simplest simulation is to neglect the convection and diffusion terms entirely, this does not produce a result consistent with the requirement that the sum of the normal stress terms obtained from the truncated equation add up to 2k, except in a special case. Rodi thus proposes the simulation

$$(\text{conv.} - \text{diff.}) \text{ of } \overline{u_i u_j} = \frac{u_i u_j}{k} (\text{conv.} - \text{diff.}) \text{ of } k$$

Rodi tested this approach on the prediction of the normal stress level in free boundary layer flows, including a mixing layer, plane jet, and plane wake. The predictions of the normal stress using this approach are in some cases better than that achieved using the full Reynolds stress approach; however, for these computations Rodi did not couple the modeled Reynolds stress equation to the momentum equation: that is, the shear stress in the momentum equation was evaluated through an effective viscosity hypothesis and not using the Reynolds stresses. Nonetheless, the relative simplicity of this approach is such that its use in the engineering calculation of recirculating flows should be further investigated.

Although the application of the Rodi algebraic stress model to planar, two-dimensional elliptic flows is relatively straightforward, the equation system for axisymmetric elliptic flows becomes relatively complex. Since it does not appear that these equations have previously been derived, the equation set is reproduced here in its entirety. The stress terms appear in the equations of motion as first derivatives, reflecting their derivation from the convection terms of the Navier-Stokes equation under Reynolds-averaging, and they can thus be numerically modeled as source terms. However, following a suggestion of Launder's, they are modeled here as diffusion terms, with non-isotropic turbulent eddy viscosities, to facilitate their use in numerical solution procedures. The governing equations are

Continuity

$$\frac{\partial(\rho U)}{\partial x} + \frac{1}{r}\frac{\partial}{\partial r}(\rho V r) = 0 \tag{11}$$

x-Momentum

$$\frac{\partial(\rho U^2)}{\partial x} + \frac{1}{r}\frac{\partial}{\partial r}(\rho r U V) = \frac{\partial}{\partial x}\left(\mu_u \frac{\partial U}{\partial x} - \frac{1}{2}\mu_{uv}\frac{\partial V}{\partial x}\right) + \frac{4}{3}\frac{1}{r}\frac{\partial}{\partial r}\left[r\left(\mu_v \frac{\partial U}{\partial r} - \mu_{uv}\frac{V}{r}\right)\right]$$

$$- \frac{1}{2}\frac{\partial}{\partial x}\left(\mu_v \frac{\partial V}{\partial r} + \mu_w \frac{V}{r} - 2\mu_{uv}\frac{\partial U}{\partial r}\right) + \frac{4}{3}\frac{1}{r}\frac{\partial}{\partial r}\left[\mu_u r \frac{\partial V}{\partial x}\right] - \frac{\partial}{\partial x}\left(P + \frac{2}{3}\rho k\right) \tag{12}$$

r-Momentum

$$\frac{\partial(\rho UV)}{\partial x} + \frac{1}{r}\frac{\partial}{\partial r}(r\rho V^2) = \frac{1}{r}\frac{\partial}{\partial r}\left[r\left(\mu_v\frac{\partial V}{\partial r} - \frac{1}{2}\mu_{uv}\frac{\partial U}{\partial r}\right)\right] + \frac{4}{3}\frac{\partial}{\partial x}\left(\mu_u\frac{\partial V}{\partial x} - \mu_{uv}\frac{V}{r}\right)$$

$$- \frac{1}{2}\frac{1}{r}\frac{\partial}{\partial r}\left[r\left(\mu_u\frac{\partial U}{\partial x} + \mu_w\frac{V}{r} - 2\mu_{uv}\frac{\partial V}{\partial x}\right)\right] + \frac{4}{3}\frac{\partial}{\partial x}\left(\mu_v\frac{\partial U}{\partial r}\right)$$

$$+ \frac{1}{2r}\left[\mu_u\frac{\partial U}{\partial x} + \mu_v\frac{\partial U}{\partial r} - 2\mu_w\frac{V}{r} + \mu_{uv}\left(\frac{\partial U}{\partial r} + \frac{\partial V}{\partial x}\right)\right] - \frac{\partial}{\partial r}\left(P + \frac{2}{3}\rho k\right) \qquad (13)$$

where

$$\mu_u = \Gamma_t\,(e_u + 1) \qquad \Gamma_t = \frac{1}{2}\rho\lambda\frac{k^2}{\varepsilon}$$

$$\mu_v = \Gamma_t\,(e_v + 1) \qquad \lambda = (1 - \alpha)/w\left[1 + \frac{1}{w}\left(\frac{P_k}{\varepsilon} - 1\right)\right]$$

$$\mu_w = \Gamma_t\,(e_w + 1) \qquad \alpha = 0.4$$

$$\mu_{uv} = \Gamma_t\, e_{uv} \qquad w = 2.5$$

Turbulent Kinetic Energy

$$\frac{\partial(\rho Uk)}{\partial x} + \frac{1}{r}\frac{\partial}{\partial r}(\rho Vkr) = \frac{\partial}{\partial x}\left(\mu_{ku}\frac{\partial k}{\partial x} + \mu_{kuv}\frac{\partial k}{\partial r}\right)$$

$$+ \frac{1}{r}\frac{\partial}{\partial r}\left[r\left(\mu_{kv}\frac{\partial k}{\partial r} + \mu_{kuv}\frac{\partial k}{\partial x}\right)\right] + P_k - \rho\varepsilon \qquad (14)$$

$$P_k = -\rho k\left[e_{uv}\left(\frac{\partial U}{\partial r} + \frac{\partial V}{\partial x}\right) + (e_u + 1)\frac{\partial U}{\partial x} + (e_v + 1)\frac{\partial V}{\partial r} + (e_w + 1)\frac{V}{r}\right]$$

Dissipation Rate

$$\frac{\partial(\rho U\varepsilon)}{\partial x} + \frac{1}{r}\frac{\partial}{\partial r}(\rho V\varepsilon r) = \frac{\partial}{\partial x}\left(\mu_{\varepsilon u}\frac{\partial \varepsilon}{\partial x} + \mu_{\varepsilon uv}\frac{\partial \varepsilon}{\partial r}\right)$$

$$+ \frac{1}{r}\frac{\partial}{\partial r}\left[r\left(\mu_{\varepsilon v}\frac{\partial k}{\partial r} + \mu_{\varepsilon uv}\frac{\partial \varepsilon}{\partial x}\right)\right] + \frac{\varepsilon}{k}\left(C_{\varepsilon 1}P_k - C_{\varepsilon 2}\rho\varepsilon\right) \qquad (15)$$

where

$$\mu_{ku} = C_s \frac{\rho k^2}{\varepsilon} (e_u + 1) \qquad \mu_{\varepsilon u} = \frac{C_\varepsilon}{C_s} \mu_{ku}$$

$$\mu_{kv} = C_s \frac{\rho k^2}{\varepsilon} (e_v + 1) \qquad \mu_{\varepsilon v} = \frac{C_\varepsilon}{C_s} \mu_{kv}$$

$$\mu_{kuv} = C_s \frac{\rho k^2}{\varepsilon} e_{uv} \qquad \mu_{\varepsilon uv} = \frac{C_\varepsilon}{C_s} \mu_{kuv}$$

$$C_s = 0.25 \quad C_\varepsilon = 0.15 \quad C_{\varepsilon 1} = 1.45 \quad C_{\varepsilon 2} = 1.9$$

These equations are closed by a set of four algebraic normal stress relations,

$$e_u = \frac{3}{2} \frac{\widetilde{u^2}}{k} = \gamma \left[(e_u + 1) \frac{\partial U}{\partial x} - \frac{1}{2} (e_v + 1) \frac{\partial V}{\partial r} - \frac{1}{2} (e_w + 1) \frac{V}{r} + e_{uv} \left(\frac{\partial U}{\partial r} - \frac{1}{2} \frac{\partial V}{\partial x} \right) \right]$$

$$e_v = \frac{3}{2} \frac{\widetilde{v^2}}{k} = \gamma \left[- \frac{1}{2} (e_u + 1) \frac{\partial U}{\partial x} + (e_v + 1) \frac{\partial V}{\partial r} - \frac{1}{2} (e_w + 1) \frac{V}{r} + e_{uv} \left(\frac{\partial V}{\partial x} - \frac{1}{2} \frac{\partial U}{\partial r} \right) \right]$$

$$e_w = \frac{3}{2} \frac{\widetilde{w^2}}{k} = \gamma \left[- \frac{1}{2} (e_u + 1) \frac{\partial U}{\partial x} - \frac{1}{2} (e_v + 1) \frac{\partial V}{\partial r} + (e_w + 1) \frac{V}{r} - e_{uv} \left(\frac{\partial U}{\partial r} + \frac{\partial V}{\partial x} \right) \right]$$

$$e_{uv} = \frac{3}{2} \frac{\overline{uv}}{k} = \frac{4}{3} \gamma \left[(e_v + 1) \frac{\partial U}{\partial r} + (e_u + 1) \frac{\partial V}{\partial x} - e_{uv} \frac{V}{r} \right] \qquad (16)$$

to be solved simultaneously, where

$$\gamma = - \frac{3}{4} \lambda \frac{k}{\varepsilon}$$

and

$$\widetilde{u^2} = \overline{u^2} - \frac{2}{3} k$$

$$\widetilde{v^2} = \overline{v^2} - \frac{2}{3} k$$

$$\widetilde{w^2} = \overline{w^2} - \frac{2}{3} k$$

2.4 MULTIPLE-SCALE MODELING

While reasonably good results have been achieved with the two-equation model in a variety of flows, including boundary layer flows and recirculating flowfields (Refs. 11, 12), several problems in its application exist. One of these is the round-jet problem: the simple configuration of the jet into still air cannot be modeled correctly while using the same constants used to model other flows, such as plane jets and coaxial axisymmetric jets. Further, the far wake problem and the effects of compressibility have not been adequately handled. In each case, the treatment of the dissipation rate is of paramount importance, and recent work by Launder and co-workers (Refs. 3, 4, 5) has pointed to a possible solution to this problem.

The key to the new multiple-scale approach is the recognition that while the dissipation equation (Eq. 10) and the kinetic energy equation (Eq. 9) both contain production and dissipation terms, these processes occur in different spectral regions of the flow. That is, turbulence energy production occurs in the larger eddies in the flow, while dissipation phenomena involve primarily the smaller scales. Thus, there must be a transfer of energy from the larger scales to the smaller, and this transfer can, in certain situations, introduce a lag phenomenon, so that turbulence energy production and turbulence energy dissipation do not necessarily both increase or decrease in the same region of the flow as is implied by Eqs. 9 and 10.

To introduce a model in which the evolution of the different scales appropriate to the large-eddy production region and the small-eddy dissipation region can be accounted for, Launder and co-workers introduced a partitioning of the turbulence energy and its dissipation rate, as shown schematically in Figure 2-1. In this figure, a partitioning into three regions is shown. For wave numbers less than κ_1, a production region is defined, characterized by a turbulent kinetic energy k_p and a dissipation rate ε_p. This dissipation affects the transfer of energy through the transfer region $\kappa_1 < \kappa < \kappa_2$; for wave numbers higher than κ_2, dissipation of turbulence energy into heat takes place. A separate kinetic energy and dissipation rate equation is written for the transfer region, characterized by k_T and ε_T, and the production term in the kinetic energy equation for the transfer region is the production region dissipation rate ε_p.

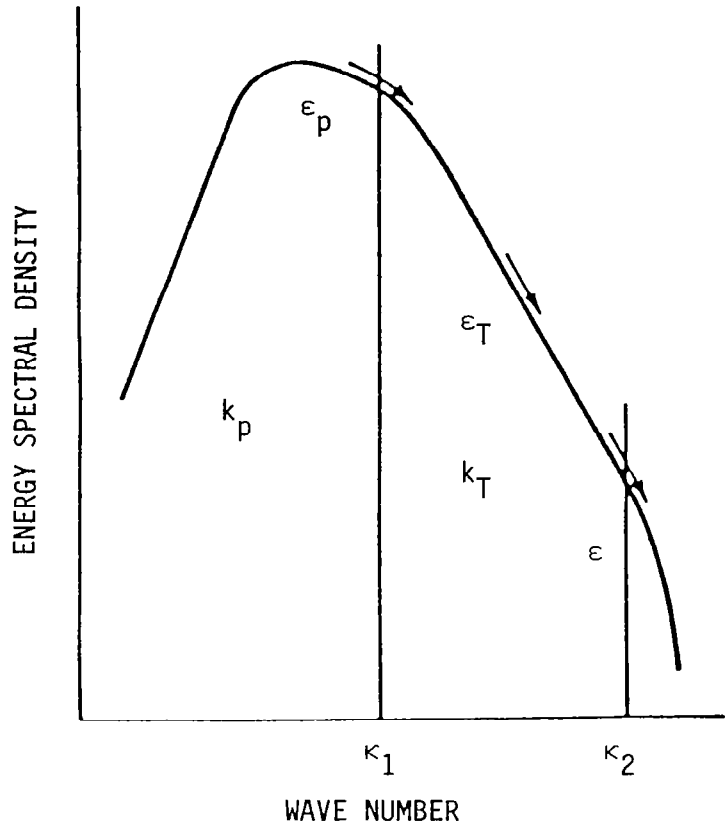

Fig. 2-1. Spectral Division of Turbulence Energy and Dissipation Rate

The partitioning of the energy spectrum that is the key feature of the multiple-scale model can clearly be carried out as many times as computer capacity will allow, but in practice, a partitioning into three regions appears to be sufficient (Refs. 4, 5). This requires two sets of transport equations, given the assumption (basic to most turbulence modeling) that the mechanisms involved in the final dissipation of turbulent kinetic energy into thermal energy are capable of accepting all of the energy transferred to them. This assumption is the reason that the physical fluid viscosity does not appear in the turbulence dissipation rate equations and is supported by the observed Reynolds number invariance of fully-turbulent flows. Further, in practice it also is observed that the exact point in the wave-number spectrum at which the

energy spectrum is partitioned does not appear to exert much influence on the results; however, it does appear to be influential in initial condition determination, as will be subsequently discussed.

The model equations, for axisymmetric parabolic flow, for the production and transfer region turbulent kinetic energy and dissipation rate are similar in form to those used in the two-equation model. The development of these equations is discussed in some detail in References 3-5; they are:

Production Region

$$\rho U \frac{\partial k_p}{\partial x} + \rho V \frac{\partial k_p}{\partial r} = \frac{1}{r} \frac{\partial}{\partial r} \left(\frac{\mu_T}{\sigma_{k_p}} \frac{\partial k_p}{\partial r} \right) + \mu_T \left(\frac{\partial U}{\partial r} \right)^2 - \rho \varepsilon_p - \rho \left(\frac{k_p + k_T}{3} \right) \frac{\partial U}{\partial x} \tag{17}$$

$$\rho U \frac{\partial \varepsilon_p}{\partial x} + \rho V \frac{\partial \varepsilon_p}{\partial r} = \frac{1}{r} \frac{\partial}{\partial r} \left(\frac{\mu_T}{\sigma_{\varepsilon_p}} \frac{\partial \varepsilon_p}{\partial r} \right) + C_{p1} \mu_T \left(\frac{\partial U}{\partial r} \right)^2 \frac{\varepsilon_p}{k_p} - \rho C_{p2} \frac{\varepsilon_p^2}{k_p} + \rho C'_{p1} k_p \left(\frac{\partial U}{\partial r} \right)^2 \tag{18}$$

Transfer Region

$$\rho U \frac{\partial k_T}{\partial x} + \rho V \frac{\partial k_T}{\partial r} = \frac{1}{r} \frac{\partial}{\partial r} \left(\frac{\mu_T}{\sigma_{k_T}} \frac{\partial k_T}{\partial r} \right) + \rho \varepsilon_p - \rho \varepsilon_T \tag{19}$$

$$\rho U \frac{\partial \varepsilon_T}{\partial x} + \rho V \frac{\partial \varepsilon_T}{\partial r} = \frac{1}{r} \frac{\partial}{\partial r} \left(\frac{\mu_T}{\sigma_{k_T}} \frac{\partial \varepsilon_T}{\partial r} \right) + \rho C_{T1} \frac{\varepsilon_p \varepsilon_T}{k_T} - \rho C_{T2} \frac{\varepsilon_T^2}{k_T} \tag{20}$$

in which the subscript p refers to the production region and T to the transfer region. In this formulation, the turbulent viscosity is given by

$$\mu_T = \rho C_\mu (k_p + k_T) \frac{k_p}{\varepsilon_p} \tag{21}$$

This formulation introduces six coefficients, compared to three for the two-equation model, but values for several of these coefficients can be inferred from two-equation model results and from examination of limiting cases. The procedure used to establish the coefficients is described in detail in Ref. 5;

the results are

$$\left.\begin{aligned} C_{p1} = 2.2,\ C_{p2} &= 1.8 - 0.3\left[\left(\frac{k_p}{k_T} - 1\right)\Big/\left(\frac{k_p}{k_T} + 1\right)\right] \\ C_{T1} &= 1.08\,\frac{\varepsilon_p}{\varepsilon_T},\ C_{T2} = 1.15 \\ C'_{p1} &= -0.11,\ C_{\mu} = 0.10 \end{aligned}\right\} \quad (22)$$

In addition to the modeling required to represent the multiple-scale approach, these equations also introduce additional modeled expressions. Thus, Eq. 17 contains the usual convection, diffusion, production, and dissipation terms; but in addition, the last term represents production of turbulence due to axial velocity gradients (which is of noticeable importance only in jet flows). Further, Eq. 18, for the production region dissipation rate, includes a term (the last term on the right-hand side) which accounts (indirectly) for turbulence energy generation by irrotational strain (Ref. 5). This term vanishes in an irrotational flow and is otherwise negative. These additional terms are not fundamental to the multiple-scale model and have been applied to improvement of the basic two-equation approach with good results (Ref. 14).

It has long been observed that there are certain "pathological" flows which available turbulence models are unable to adequately represent. One of these is the flowfield that results when a grid-generated decaying turbulent wake flow is passed through a contraction section. During this process, the kinetic energy is observed to increase and then decay again, but at a slower rate than before. Two-equation model predictions either underpredict the secondary peak achieved and the subsequent rate of decay, or overpredict both, depending on the coefficients selected: proper prediction of both the secondary peak energy level and the subsequent rate of decay seems to be beyond the capability of the basic two-equation model. The multiple-scale model does successfully predict this flow, and study of the calculation results of this flowfield (taken from Ref. 5) provides further insight into the behavior of the multiple-scale model.

Figure 2-2 shows the results of two-equation and multiple-scale model computations of the turbulent kinetic energy level of a decaying wake flow passed through a 4:1 contraction, compared to the measured data for this flow (Ref. 5).

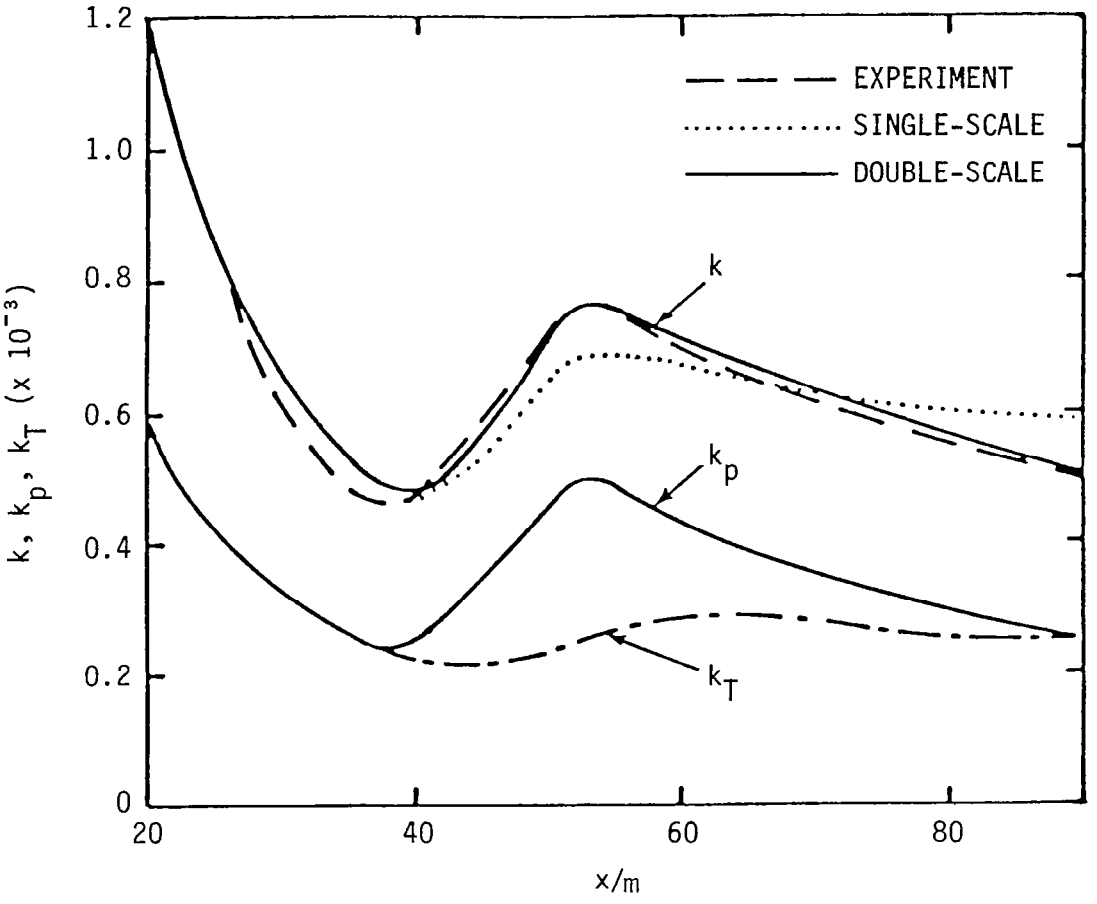

Fig. 2-2. Development of Kinetic Energies in 4:1 Contraction (Ref. 5)

Clearly, the multiple-scale (here "double-scale") model provides a very good representation of this flowfield, one that is considerably better than that produced by the basic two-equation ("single-scale") model. Of additional interest is the manner in which this improvement is achieved. In the single-scale approach, the increase in kinetic energy would immediately result in an increase in the dissipation rate of turbulent kinetic energy. For the multiple-scale approach, the division of the energy spectrum into a production region

and a transfer region introduces a lag in the increase in dissipation rate. As can be seen from Figure 2-3, the increase in production region kinetic energy is, as in the two-equation formulation, accompanied by an increase in production region dissipation rate. But instead of being lost from the turbulence energy budget, as would be predicted by the two-equation model, this energy is transferred to a different spectral region. The ultimate transfer of this energy to the smaller scales which produce dissipation of turbulence energy into thermal energy lags the transfer of energy from the production region to the transfer region, as can be seen from Figure 2-3. This results in the higher peak energy and subsequent rapid decay seen in Figure 2-2.

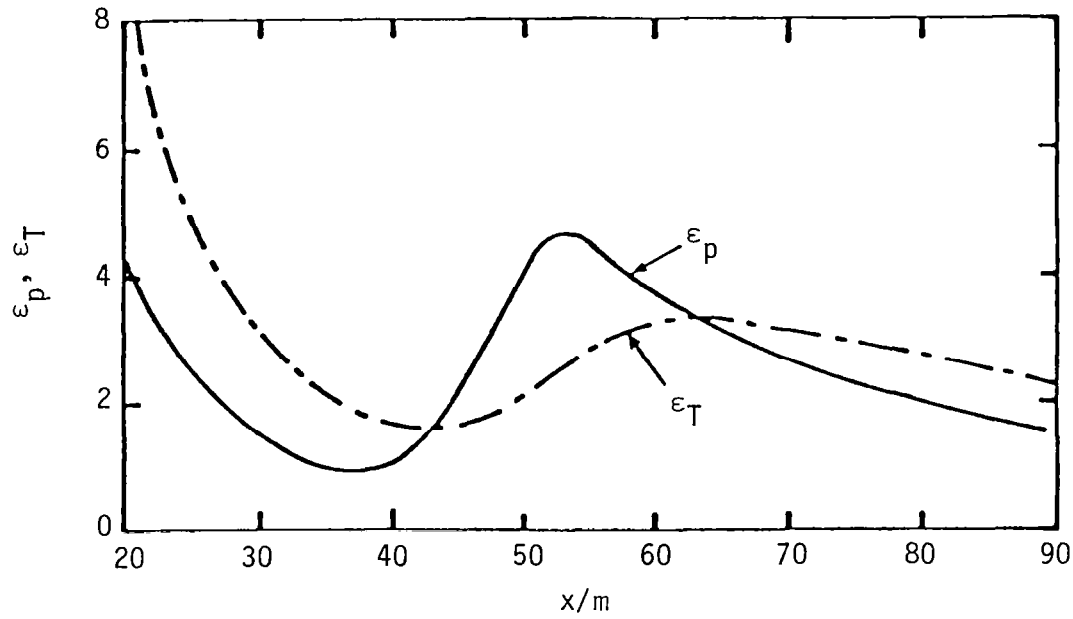

Fig. 2-3. Development of Energy Transfer Rates Through 4:1 Contraction (Ref. 5)

Thus, the basis of the multiple-scale approach can be described through the use of a "tank-and-tube" analogy as shown in Figure 2-4 (Ref. 5). The dissipation rate, ε_p serves as a "valve" controlling the transfer of energy from the production "tank" to the transfer "tank"; the loss of energy from the transfer "tank" is defined by the dissipation rate ε_T, which by definition is

equal to the rate of conversion of turbulence energy to thermal energy. Production of turbulence, P_k, which occurs in the larger eddies, feeds into the production region "tank" and not the transfer region. For relatively simple flows, in which the basic two-equation model performs well, $\varepsilon_p \simeq \varepsilon_T \simeq \varepsilon$, so that there is little or no energy buildup in the transfer region. But for more complex flows, ε_p and ε_T are not equal, and turbulent kinetic energy is transferred from the production region to the dissipation region, but not immediately destroyed.

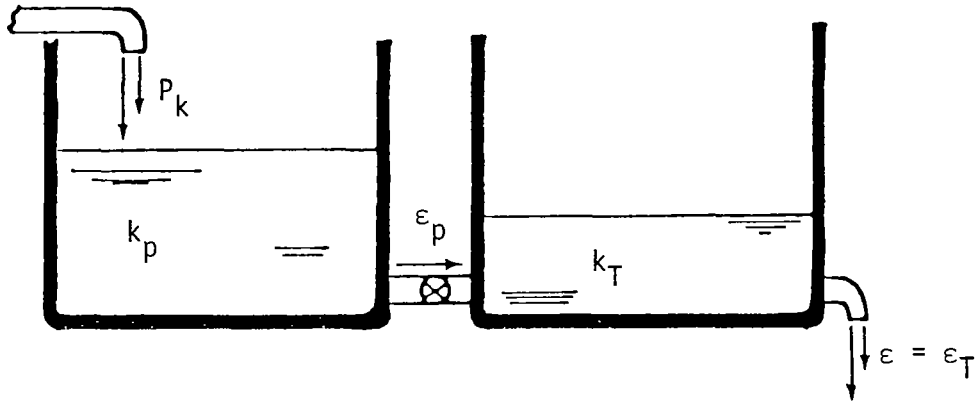

Fig. 2-4. Tank-and-Tube Analogy of Spectral Transfer of Energy

The multiple scale approach has several advantages in the context of scramjet combustor modeling. Scramjet flowfields involve localized regions of strong pressure gradients, which are known to severely affect local turbulence levels. Thus, a model which predicts the behavior of a turbulent flow passing through a strong pressure gradient associated with waves and wave interaction and regions of fuel injection and ignition is potentially more accurate and reliable than the two-equation model for scramjet applications. Moreover, as pointed out in the Introduction, the multiple-scale approach offers the possibility of the development of deterministic relations for unmixedness effects important in modeling ignition and flame stabilization phenomena. However, before proceeding with the use of the multiple-scale approach, its reliability needs to be established: how well does the model perform for a variety of flowfields, all

of which can be encountered in scramjet combustors? Further, the multiple-scale approach requires more detailed initial conditions than does the two-equation approach, and if it is to be utilized in an engineering model, reliable methods for estimating these initial conditions need to be determined.

3. RESULTS OF MULTIPLE-SCALE MODEL COMPUTATIONS

In order to establish the accuracy and reliability of the multiple-scale turbulence model approach, and to develop a reliable method for initial condition specification for this model, an extensive series of computations and comparisons with available experimental data have been carried out. Most of the data used in this comparison are those used for comparison with computations at the 1972 NASA-Langley Symposium on Turbulent Shear Flows (Ref. 16). These data have been utilized for several reasons: the symposium committee selected these cases as the most suitable for comparison purposes after an exhaustive survey of available data; they represent a variety of flowfields most of which are highly relevant to scramjet combustor applications; and comparison with these data provides a ready reference point for comparison of predictions of the multiple-scale model with other turbulence model approaches. Other data have also been incorporated into the comparisons reported in this section, where appropriate either because of certain questions which exist with regard to some of the data used in the 1972 Langley Symposium or because the particular configuration of interest was not included in the Symposium flows. Throughout this section, comparisons of multiple-scale model predictions with those of the "standard" two-equation model are reported. For these comparisons, the two-equation model results described in Ref. 16 were not used. Instead, the two-equation model results presented in this section were obtained using the same computer code and initial condition determination technique utilized for the multiple-scale model.

The calculation technique utilized for all of the parabolic flowfield solutions described in this section is based on the explicit finite-difference code described by Boccio, et al. in Ref. 17. This code solves the equations of motion in stream function coordinates and is capable of computing planar or axisymmetric, free or ducted turbulent flow phenomena for incompressible or compressible flows. For use in this work, the code was slightly modified to

allow input of initial profiles in physical rather than stream function coordinates and to incorporate both the two-equation and multiple-scale turbulence models. Elliptic flowfield calculations for the recirculating, sudden-expansion flowfield case used an implicit finite-difference code similar to the Imperial College TEACH formulation (Ref. 18). In this case, it was found necessary to use a fine, 25 x 100 computational grid to ensure adequate freedom from numerical diffusion effects to provide a test of the turbulence model formulation. About 1000 iterations were required with this degree of grid fineness to obtain a stable solution in terms of predicted recirculation zone length.

3.1 INITIAL CONDITION DETERMINATION

A central issue with regard to the use of advanced turbulence models for the prediction of flowfields of engineering interest is the development of techniques for the accurate estimation of initial conditions and the sensitivity of the model itself to the initial conditions. This issue arises because the more general turbulence models involve the solution of turbulence transport equations reflecting the evolution of the turbulence structure. These more realistic models require more detailed initial condition data. However, these data, for example for initial turbulent kinetic energy and dissipation rate profiles, are generally not available: certainly such detailed data cannot be expected to be available for most scramjet flowfields. On the other hand, sensitivity to initial conditions is not a true test of turbulence model performance and is seldom included in turbulence model evaluations.

Because the objective of this program is the development of turbulence models for engineering use, with certain exceptions all of the computations reported herein begin from estimated, rather than measured, initial turbulence data. In some cases, initial mean flow profiles have also been estimated. For the multiple-scale model, not only must initial turbulent kinetic energy and dissipation rate data be specified, but also the initial partition of the energy and dissipation rate into production and transfer regions. Thus, an extensive investigation of initial condition effects on flowfield predictions has been required.

An example of the sensitivity of turbulence model predictions to initial condition specification is shown in Figure 3-1. In this figure, a variety of single-scale two-equation model predictions of the downstream decay of an axisymmetric jet are shown. Computations were initiated at X/D = 60 using measured turbulent kinetic energy profiles as initial conditions; the only difference between the computations shown is the assumed dissipation rate. Model coefficients used were those shown in the figure.

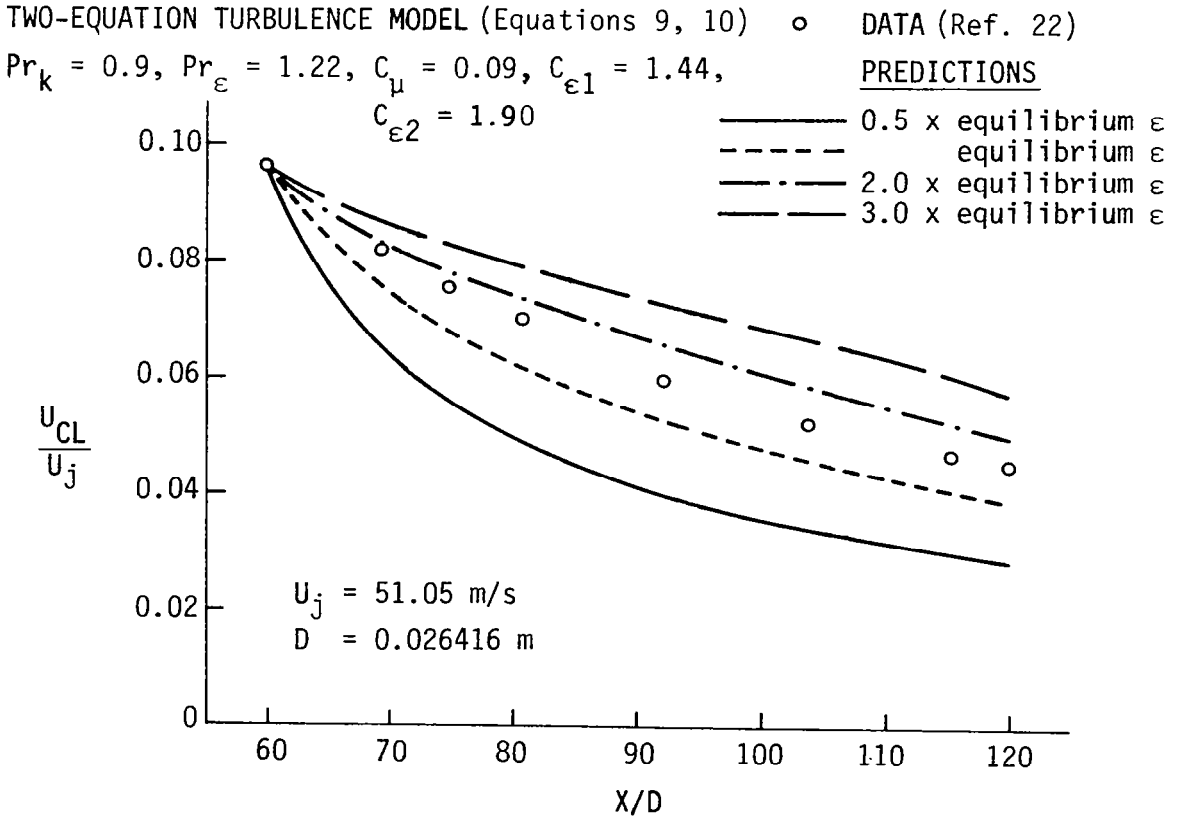

Figure 3-1. Effect of Initial Dissipation Rate on Axial Velocity Decay, Far Field of Axisymmetric Jet

The basic assumption used to generate dissipation rate initial conditions is usually taken to be that turbulence energy production equals turbulence energy dissipation rate. As these results show, for this flow this "equilibrium" assumption results in a slightly overpredicted initial centerline velocity decay rate. Other perturbations on the "equilibrium" assumption produce the other results shown in Figure 3-1. While this flowfield is especially

sensitive to initial condition specification, since by X/D = 60 the jet has progressed into a relatively weak shear region, these results indicate the level of initial condition sensitivity that can be encountered with a widely used turbulence model.

Despite the sensitivity illustrated in Figure 3-1, an extensive investigation of initial condition estimation techniques carried out as part of this program has resulted in a generalized approach that, as will be shown, provides reasonably good results for all of the flowfields considered. The technique applies to initial conditions in the strong-shear region of the flow, where the sensitivity exhibited in Figure 3-1 is somewhat reduced, as well as to initial conditions in the weak-shear region. The approach is based on the use of eddy viscosity models to generate an initial shear stress and thus kinetic energy profile, and is based on the technique devised by Harsha (Ref. 19) for use with the one-equation turbulent kinetic energy model. It can be summarized as follows:

1. Origin at nozzle exit: Maise and McDonald (Ref. 20) eddy viscosity profiles are used to establish the initial shear stress and thus the turbulent kinetic energy distribution; actual boundary layer thickness is used if reported, otherwise $\delta \simeq 0.10\ r_j$; actual boundary layer velocity profile is used if reported; otherwise a 1/7 power law boundary layer is assumed. The initial turbulent kinetic energy partition is given by $k_p = 4k_T$ (and $k_p + k_T = k$).

2. Origin in potential core region (jets) or before self-preserving region (wakes and shear layers): The Prandtl eddy viscosity model is used to establish the initial shear stress and thus turbulent kinetic energy distribution, along with measured velocity profiles. An eddy viscosity coefficient of 0.005 is used with the length scale equal to the mixing region width. The initial turbulent kinetic energy partition is assumed to be $k_p = 4k_T$.

3. Origin in self-preserving region: The measured velocity and, if available, turbulent kinetic energy profiles are used; otherwise the turbulent kinetic energy profiles are obtained from the Prandtl eddy viscosity model, with a coefficient of 0.014 and a length scale given by the mixing region half-width. The initial turbulent kinetic energy partition is given by $k_p = k_T$.

Once an initial eddy viscosity distribution is obtained by one of these approaches, the relation

$$|\tau| = 0.30 \rho k$$

which has been found to be supported by a wide variety of experimental data (Ref. 21) is used to obtain the kinetic energy distribution from the relation

$$k = 3.33 \frac{|\tau|}{\rho} = 3.33 \nu_T \left|\frac{\partial U}{\partial y}\right|$$

In the region of a centerline this approximation fails, since k does not approach zero on a centerline while τ does, so that for this region the initial value of k is assumed to be equal to its maximum value attained in the derived profile. Given k, the dissipation rate, ε, is obtained from an equilibrium hypothesis; for the multiple-scale model the initial partition between k_p and k_T is as outlined above, while in all cases $\varepsilon_p = \varepsilon_T$ initially.

The effect of the choice of the initial partition of the kinetic energy into production and transfer regions is shown in Figure 3-2, which, like Figure 3-1, shows results obtained for the axisymmetric jet case. For this case, as noted earlier, the initial turbulent kinetic energy is obtained from experimental data. Use of the weak-shear region partition, $k_p = k_T$ can be seen to provide a better representation of the initial decay rate than does the strong-shear partition, $k_p = 4k_T$. Neither of the initial conditions result in a proper representation of the far-field decay rate for this flow, for reasons that are discussed in the next section.

3.2 AXISYMMETRIC JETS

In this section, results of computations with both the two-equation and multiple-scale models are compared with experimental data for axisymmetric, single-gas jets. The experiments include the jet-into-still-air and two-stream coaxial jets, in the latter case both ducted and free. While these particular configurations are not directly applicable to scramjet combustor flowfields, they provide well-documented data that is suitable for a critical test of turbulence modeling. Further, single-jet experiments at different nozzle exit Mach numbers provide a test of the ability of turbulence models to predict

compressibility effects in reasonably simple flowfields, and the prediction of compressibility effects is of critical interest in the development of turbulence modeling for scramjet combustors.

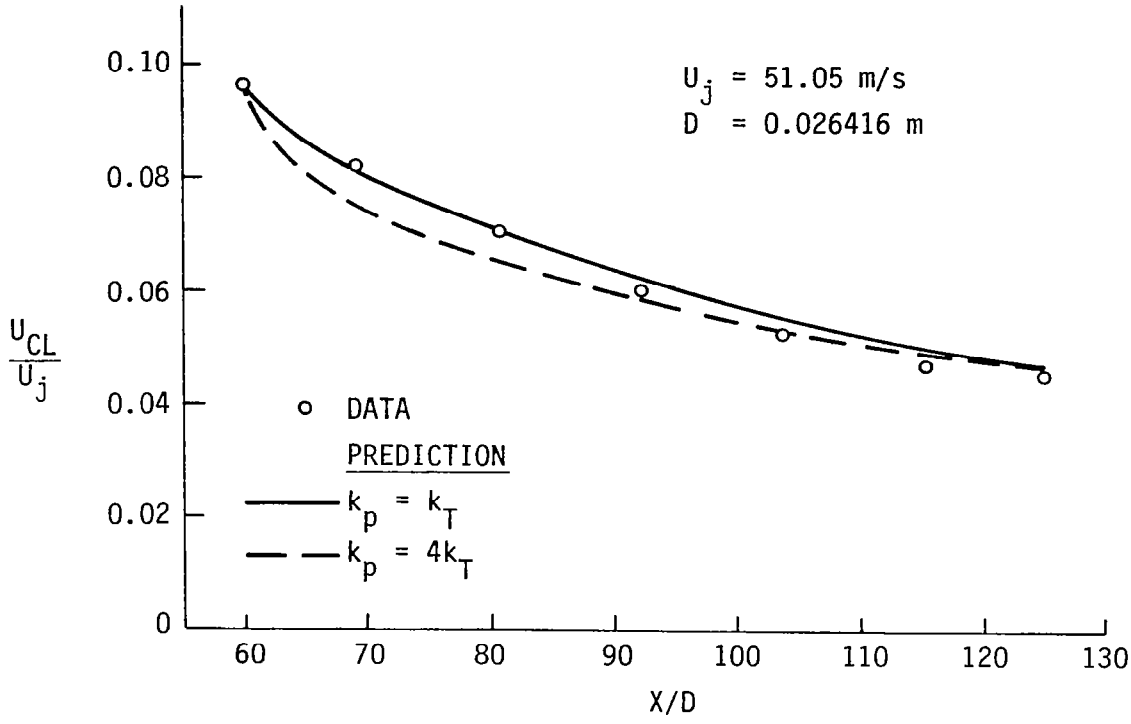

Fig. 3-2. Effect of Initial Kinetic Energy Partition on Centerline Decay Prediction, Far Field of Axisymmetric Jet

The development of an axisymmetric jet in the far field was the focus of test case 18 of the 1972 NASA Langley Symposium. These data, from Ref. 22, were obtained using a linearized constant-temperature hot wire anemometer in the self-preserving region of a free jet, X/D > 60. A variety of initial conditions are possible for this flowfield: use of the experimental data given for X/D > 60; use of other experimental data for 0 < X/D < 60; or estimated nozzle-exit initial conditions. Because of the initial condition sensitivity that has already been noted, when the computation is begun in a weak-shear region, computations for this case are initiated from experimental initial conditions reported by Bradshaw, et al. (Ref. 23) at X/D = 1, using the Prandtl eddy viscosity model to estimate the initial kinetic energy profiles.

Unfortunately, although test case 18 was selected in the 1972 NASA Langley Symposium to represent the asymptotic jet, these data exhibit an anomalous behavior, as has been noted both by Harsha (Ref. 24) and by Rodi (Ref. 25): between X/D = 60 and X/D = 70 the slope of the experimental velocity decay curve changes sharply, with concurrent changes in the overall flow momentum flux. Thus, for asymptotic jet prediction comparisons, the test case 18 data have been supplemented by the experimental data obtained by Albertson, et al. (Ref. 26) and by Baines (Ref. 27).

Turbulence model computation results for both the multiple-scale and two-equation (k-ε) models are shown in Figure 3-3 compared to all of the data noted in the preceding paragraph. For this, and all subsequent comparisons, the coefficients used with the multiple-scale model are those given by Eqs. 22; for the two-equation model the coefficients shown in Figure 3-1 have been used. Thus, no attempt has been made to use for the two-equation model the coefficients and model modifications specifically reported for axisymmetric jet flowfields. It is clear from Figure 3-3 that the multiple-scale model provides a very much better representation of far field velocity decay behavior than does the basic two-equation model, as has been reported earlier by Launder and coworkers (Ref. 4). The model also provides a good representation of near-field data, as shown in Figure 3-4, especially when it is noted that the specific initial conditions associated with the data of Refs. 26 and 27 were not used for the computations shown. The significance of this is that small differences in initial conditions (i.e., thickness and state of initial boundary layers, jet Reynolds number) have been shown (Ref. 24) to exert a marked influence on the length of the jet potential core. On an inverse velocity ratio plot such as Figure 3-4, the effect with respect to the calculated results is to change the intercept of the curve with the abscissa, but not the slope of the curve.

It should be noted that a portion of the improvement between the two-equation (k-ε) model results and those of the multiple-scale model shown in Figures 3-3 and 3-4 is traceable to the introduction of the axial gradient kinetic energy production term and the irrotational strain term in Eqs. 17 and 18. Both of these can be applied to the basic two-equation model (Ref. 14). The effects of the use of these terms on the prediction of the axisymmetric jet flowfield is shown, for the multiple-scale model, in Figure 3-5.

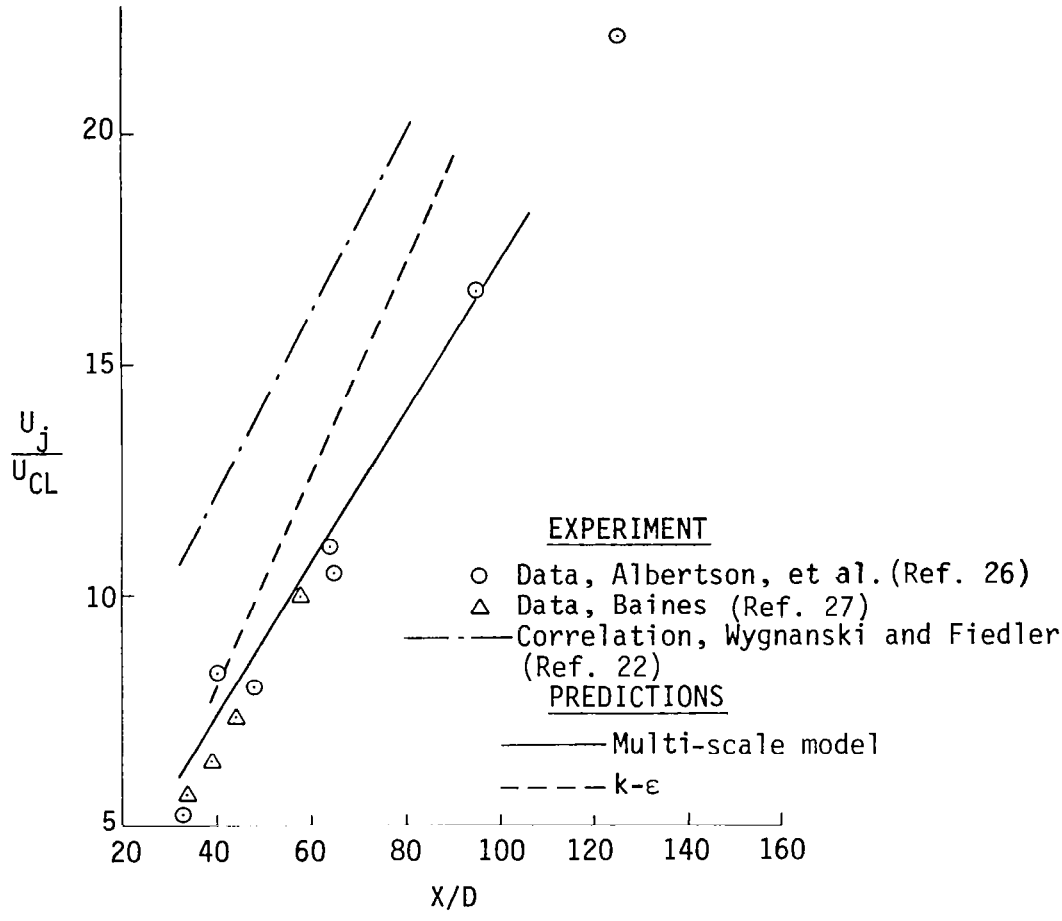

Fig. 3-3. Far Field Jet Decay Behavior

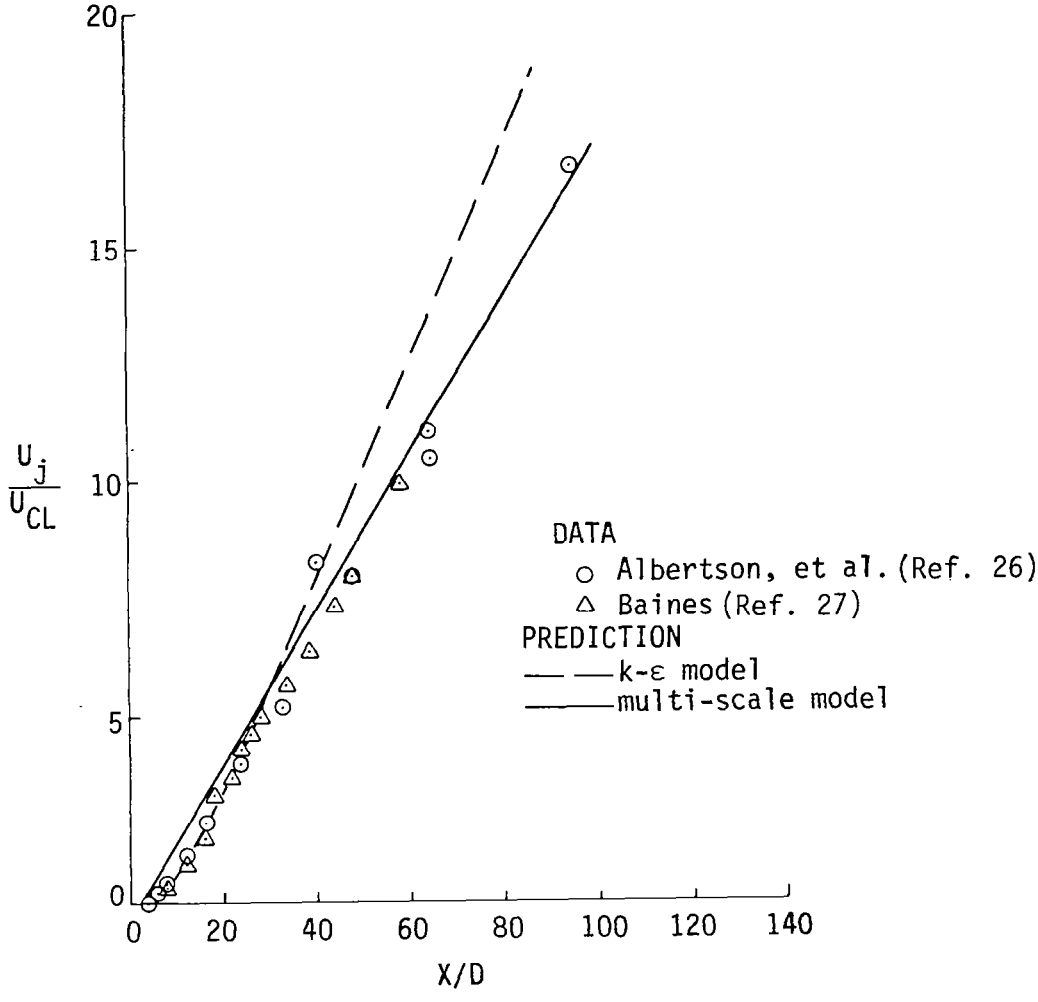

Fig. 3-4. Jet Into Still Air Comparison

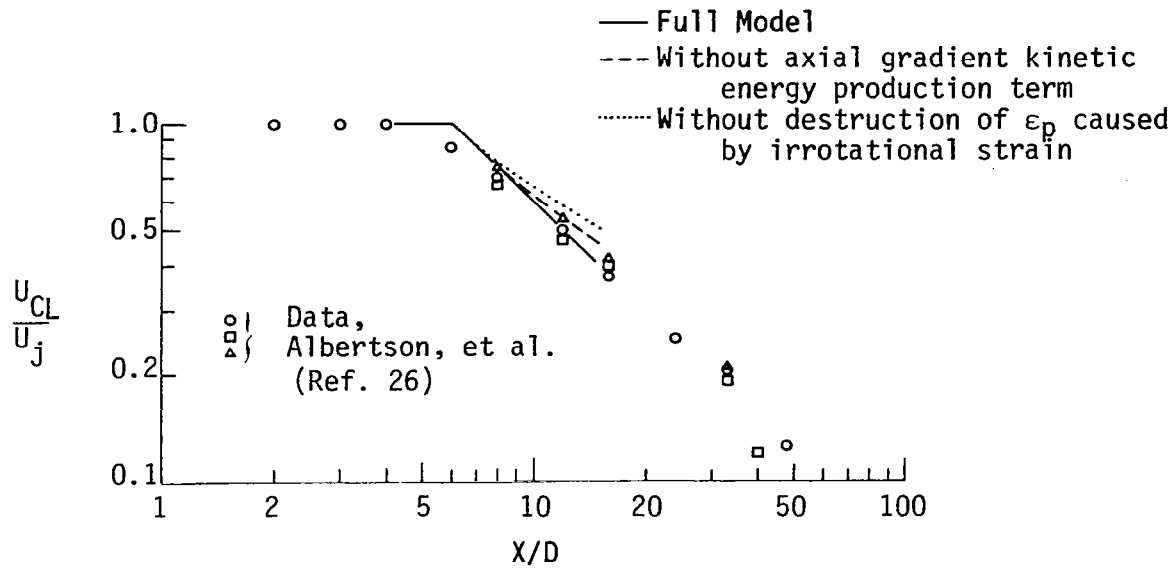

Fig. 3-5. Effects of Additional Terms, Multi-Scale Model

Test case 6 of the 1972 NASA Langley Symposium (Ref. 16) involves an axisymmetric cold jet into still air (Ref. 28) at a jet exit Mach number of about 0.6. This flowfield is thus mildly compressible. Computations for this case were initiated at X/D = 1, using the experimentally measured mean velocity profiles and the Prandtl eddy viscosity model to estimate the initial kinetic energy distribution. Results of the computations are shown in Figure 3-6, which provide a comparison of the two-equation and multiple-scale model predictions, the latter for two initial kinetic energy partitions. Both the two-equation and multiple-scale models provide a reasonable prediction of these data, when the strong-shear kinetic energy partition is used with the multiple-scale model. Use of a weak-shear partition, $k_p = k_T$, results in a drastic overprediction of the potential core length for this flow.

Both the two-equation and multiple-scale models strongly underpredict the potential core length for the supersonic jet, test case 7 of Ref. 16. These data, from Ref. 29, were obtained using a circular cross-section, Mach 2.22 nozzle designed for axial flow at the exit, operated at design pressure ratio with the jet total temperature equal to the ambient temperature. They provide a direct test of the modeling of compressibility effects: data obtained by Warren (reviewed in Ref. 24) show that the effect of increasing jet exit Mach

number (and thus also jet exit Reynolds number) for a series of fully-expanded supersonic jet experiments is an increase in the velocity potential core length. A similar effect of jet exit Reynolds number on velocity potential core length is also seen for incompressible jets, as has already been noted, but the effect for compressible flows is considerably stronger and presumably involves compressibility as well as Reynolds number effects (Ref. 24). As can be seen from Figure 3-7, neither the basic two-equation model nor the basic multiple-scale model provides a good representation of the velocity potential core length for these data, although the downstream velocity decay rate is reasonably well represented. However, it is possible to improve the observed level of agreement for the multiple-scale model through the use of a compressibility-effects correction term, as will be discussed in a subsequent section of this report.

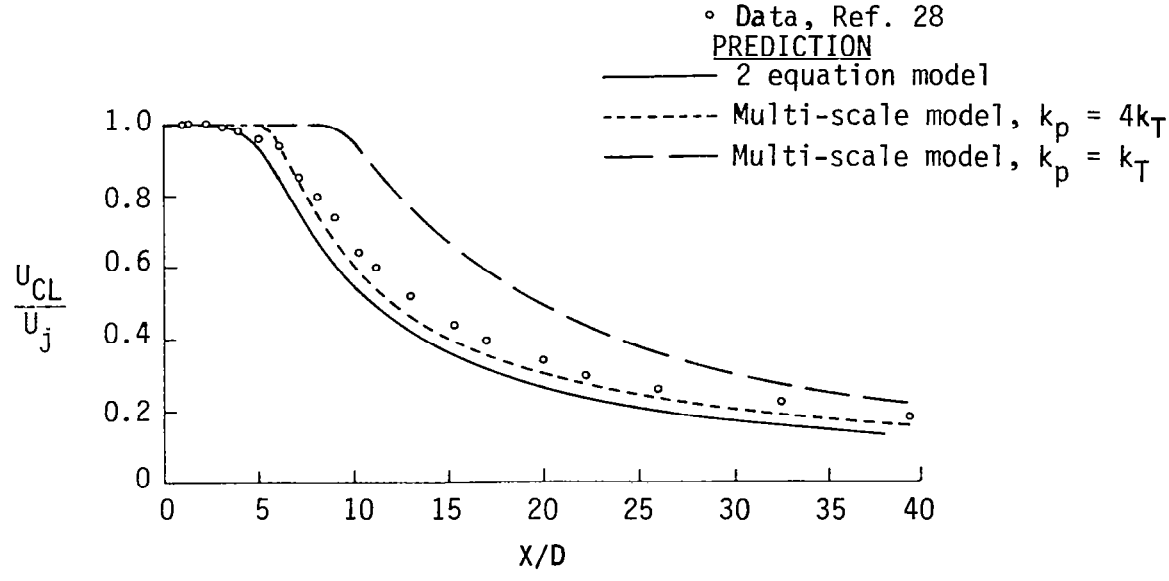

Fig. 3-6. Compressible Axisymmetric Jet

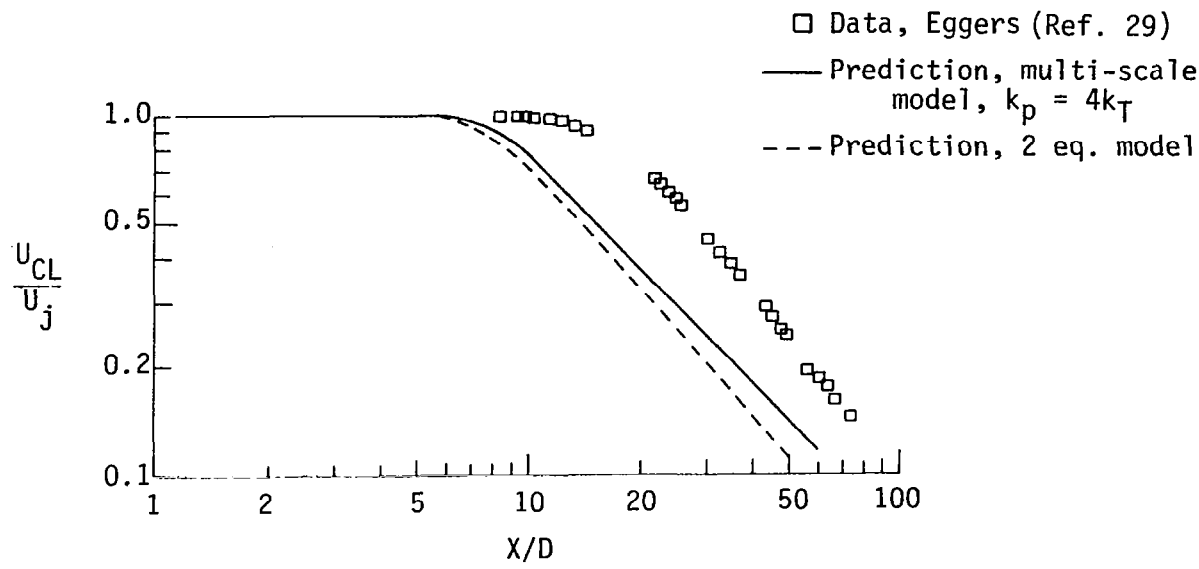

Fig. 3-7. Centerline Velocity Decay, M_j = 2.22 Jet

The mixing process involved in coaxial air jets was the subject of test case 9 of the 1972 NASA-Langley Symposium, using data reported by Forstall and Shapiro (Ref. 30). In this experiment, the mixing process occurred in a 10.2 cm-diameter (4 in.) copper tube, with an inner nozzle diameter of 0.635 cm (0.25 in.). For the test case, the velocity ratio between the outer stream and the center stream was nominally 0.25; the center stream and outer stream both involved relatively thick boundary layers at the nozzle exit. Although the flowfield was ducted, throughout the measurement region the static pressure was nominally uniform: computations made as part of this program using both constant pressure and constant wall radius boundary conditions confirmed this assumption. The initial conditions for the computations were established at the nozzle exit using the measured initial velocity profiles and eddy viscosity distribution obtained from the boundary layer data of Maise and McDonald (Ref. 20).

Results of the computations are shown in Figure 3-8, for the basic two-equation model and the multiple-scale model, the latter again with two partitions of the initial turbulent kinetic energy. For this flow, the results of the two-equation model and the multiple-scale model with $k_p = 4k_T$ nearly overlap; again the use of the weak-shear partition, $k_p = k_T$, produces an excessively long potential core.

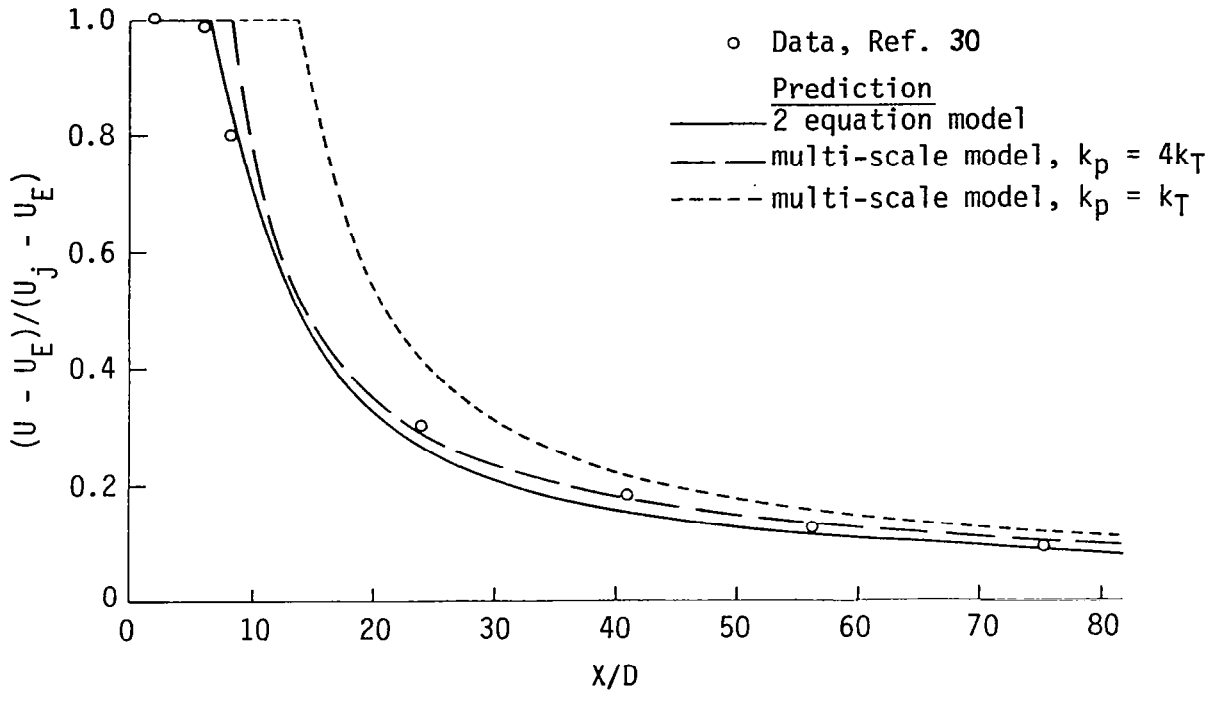

Fig. 3-8. Centerline Velocity Decay, Coaxial Jets

Test case 23 of Ref. 16 involved a relatively more complex flow than the others considered in this section. The configuration for this experiment involved coaxial jets exhausting into quiescent surroundings. The central jet was 2.64 cm (1.04 in.) in diameter and was surrounded by an annular nozzle of 5.13 cm (2.02 in.) diameter; both were mounted flush in a plane wall. The outer jet velocity was approximately 60 m/sec, and the outer jet to inner jet velocity ratio was 5.05. Thus, the centerline velocity for this case initially increases as mixing takes place between the higher and lower velocity streams, and then decreases as mixing with the quiescent surroundings proceeds. Initial conditions for these computations were established using the mean velocity profiles measured at X/D = 0.606 (based on the larger nozzle diameter) along with measured initial kinetic energy data.

As can be seen from Figure 3-9, neither the two-equation nor the multiple-scale model provide a good prediction of the initial development of this flowfield. It is again clear that the strong-shear partition is more appropriate

than the assumption $k_p = k_T$, and the downstream mixing process is well represented by both the two-equation and multiple-scale models. Radial velocity and turbulent kinetic energy profiles for the multiple-scale calculation of these data are shown in Figures 3-10 and 3-11, and it appears that at the axial station considered, the computed mixing region development is slower than that experimentally measured. This is evidenced by the reduced width of the computed velocity profile compared to the measured velocity, Figure 3-10, coupled with the overprediction of the peak turbulent kinetic energy, Figure 3-11. The measured velocity profiles show a slight off-axis peak, which is not observed in the predictions. While this difference is consistent with the higher peak kinetic energy in the predictions than shown by the data, which would result in a greater mixing rate than experimentally observed, the data for both the mean velocity and the turbulent kinetic energy appear to be shifted radially relative to the predicted profiles. Thus, there is some indication that the geometric and flowfield centerlines did not coincide for this experiment.

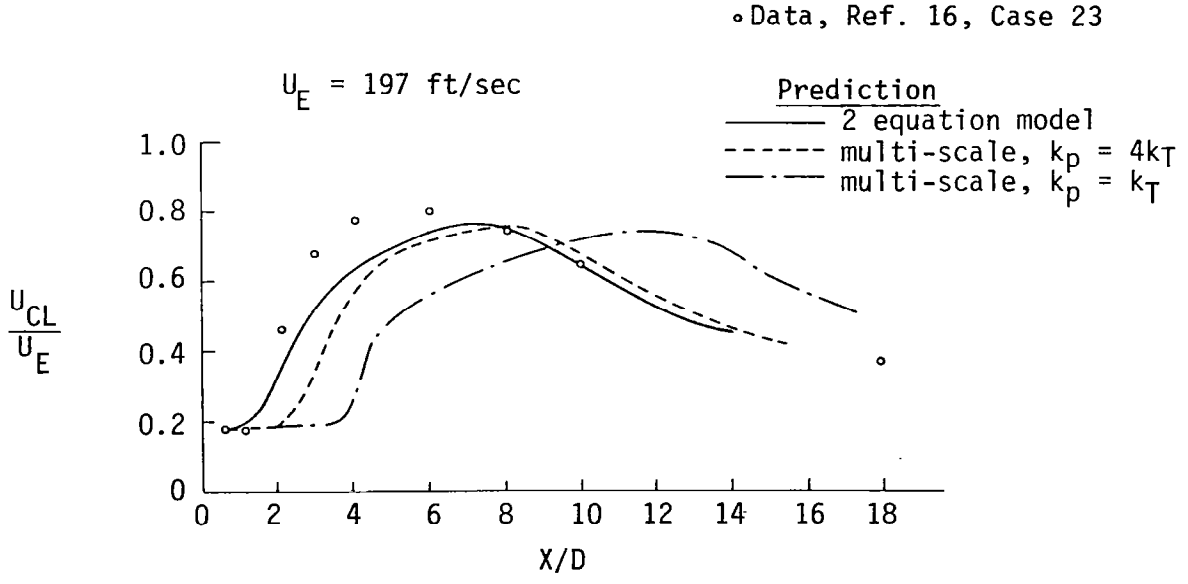

Fig. 3-9. Coannular Jet

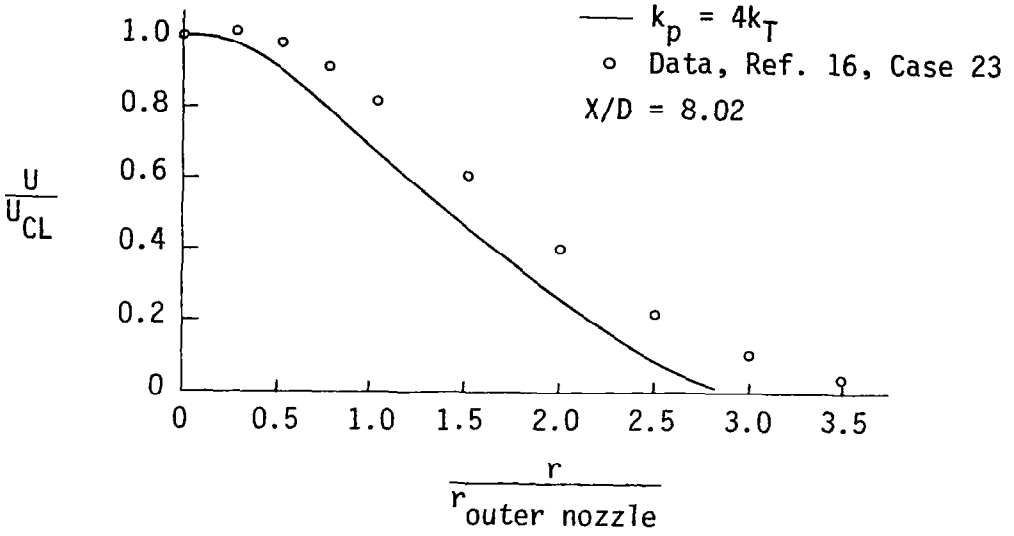

Fig. 3-10. Radial Velocity Profiles, Coannular Jet

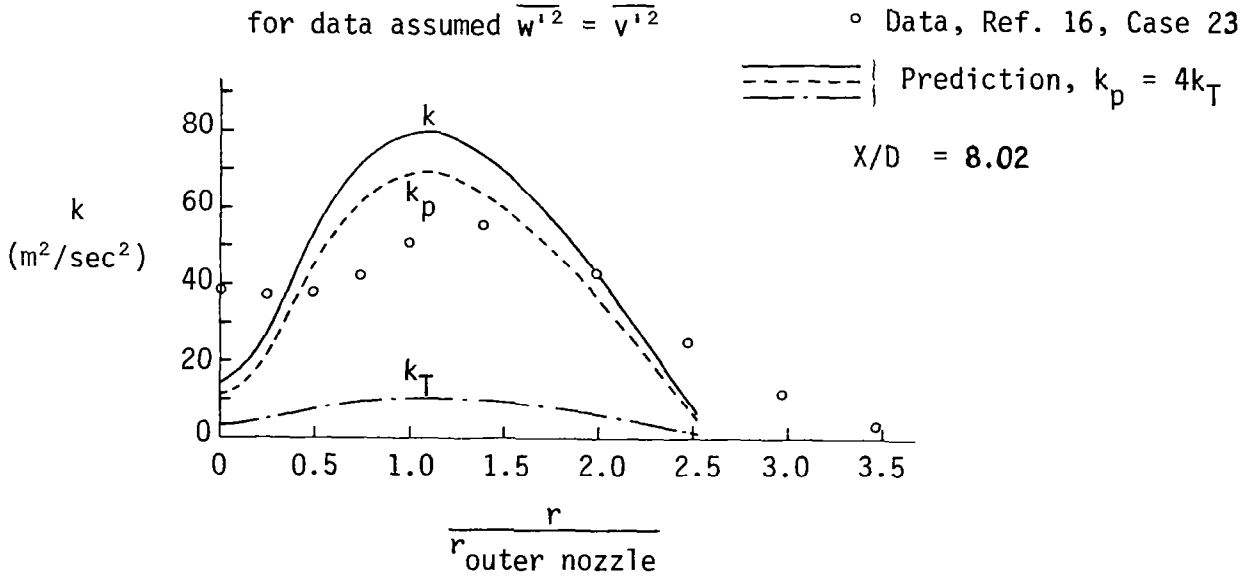

Fig. 3-11. Radial Kinetic Energy Profiles, Coannular Jet

3.3 WAKES

Supersonic wake phenomena form a basic part of a scramjet combustor flowfield and thus an examination of the performance of the multiple-scale model in predicting supersonic planar and axisymmetric wakes was undertaken. The prediction of axisymmetric incompressible wakes was also studied since, as in the case of jet phenomena, more detailed turbulence structure data is available for incompressible flows than for compressible flows.

The incompressible axisymmetric wake is represented in Ref. 18 by test case 15, which uses the data reported by Chevray (Ref. 31). The wake reported in Ref. 31 is produced by a six-to-one prolate spheroid, 1.52 m (5 ft) long, suspended in a 1.52 m (5 ft) wide octagonal cross-section low-speed wind tunnel. The free-stream velocity was about 27 m/sec (90 ft/sec). Detailed mean flow and turbulence structure data were obtained using a hot-wire anemometer. Computations of this flowfield were complicated by the existence of a recirculation region downstream of the wake-producing body, so that calculations were initiated at X/D = 1 using measured mean velocity and turbulent shear stress data. The results of this computation, using the multiple-scale model, with $k_p = 4k_T$, are shown in Figure 3-12; reasonably good agreement is achieved.

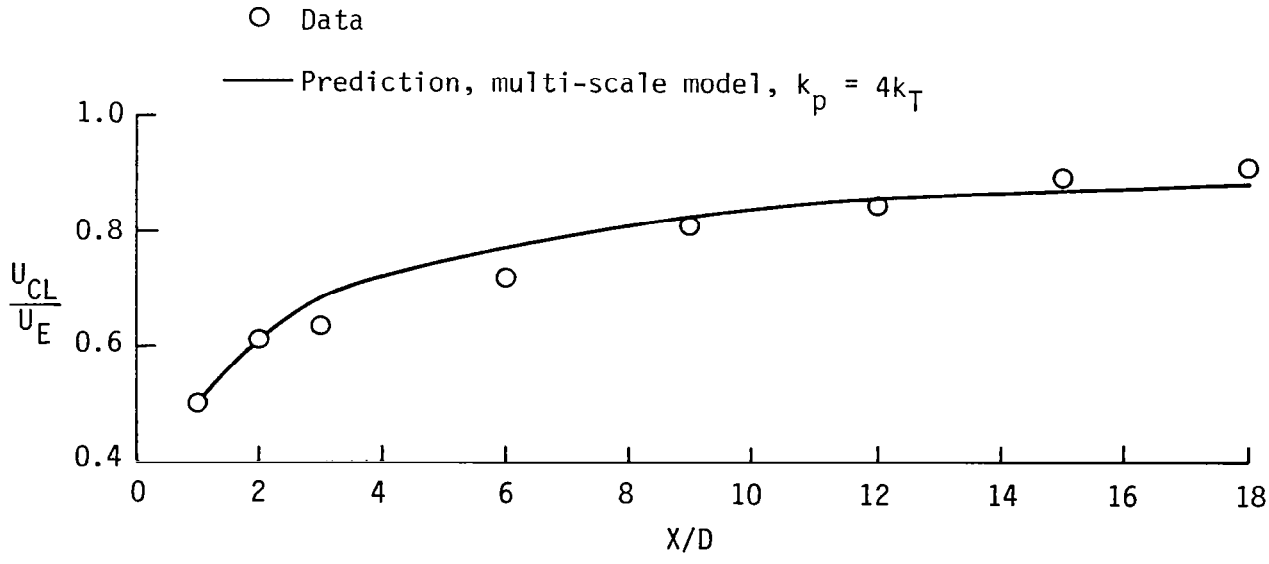

Fig. 3-12. Chevray, Axisymmetric Wake

Supersonic wake flows again introduce the phenomenon of compressibility effects, although possibly in a different manner than associated with jet flows, since in the wake case the mixing flowfield is accelerating rather than decelerating. Data for a two-dimensional supersonic wake are presented as test case 16 of Ref. 16; the wake was generated by a two-dimensional stainless steel ribbon, 0.0102 cm thick and 0.294 cm wide, stretched across a Mach 3 wind tunnel. Velocity and temperature profiles were obtained to a distance of 18.44 cm downstream of the stainless steel ribbon, yielding a nondimensional distance of 1840 thicknesses. Computations of this flowfield were begun using measured profile data of 0.91 cm downstream of the ribbon; turbulent kinetic energy profiles were estimated from the Prandtl eddy viscosity model. Results for the two-equation model and for the multiple-scale model with two initial turbulence energy partitions are shown in Figure 3-13.

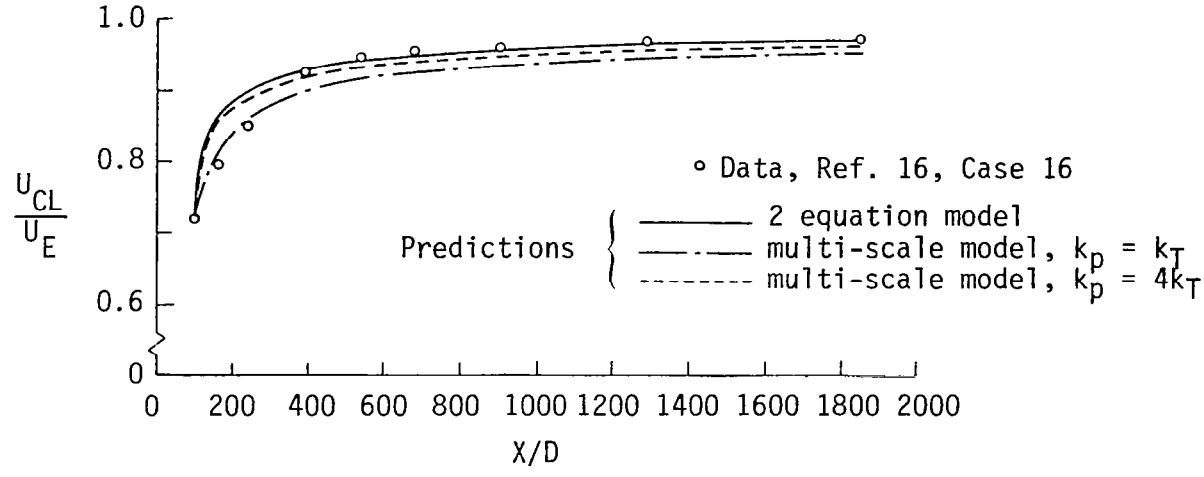

Fig. 3-13. Comparison of Model Predictions With 2D Supersonic Wake Data

A companion experiment to that just described is represented by test case 17 of Ref. 16. In this case, an axisymmetric wake was generated by the boundary layer formed on a rod, 0.4 cm in diameter, suspended in a Mach 3 wind tunnel. The supports of the rod were upstream of the nozzle throat, and test conditions were such as to yield a laminar boundary layer on the rod, with transition occurring in the wake close to the base of the rod. The first survey was carried out 17 diameters from the base, and surveys were carried out

to about 60 diameters downstream. As for the two-dimensional wake, computations were initiated using the measured mean velocity profiles and turbulent kinetic energy profiles generated using the Prandtl eddy viscosity model.

Computational results obtained using both the two-equation and multiple-scale models are shown in Figure 3-14. For this case, the equilibrium hypothesis, $k_p = k_T$ was used to obtain the initial energy partition. Comparing these results with the planar wake results shown in Figure 3-13, it can be concluded that the use of a strong-shear partition, $k_p = 4k_T$, would produce results closer to those of the basic two-equation model. It is of interest to note that for both the two-dimensional and axisymmetric supersonic wakes, the predictions are most in disagreement with the data early in the computation, where Mach number profiles across the stream are largest. In part, this observation is caused by the method of plotting, since both experiment and prediction must become asymptotic to a velocity ratio of 1.0 as distance increases. Nevertheless, this can be taken to indicate that compressibility effects may be describable by relative, rather than absolute Mach numbers, or by an approach that considers Mach number gradients across the stream.

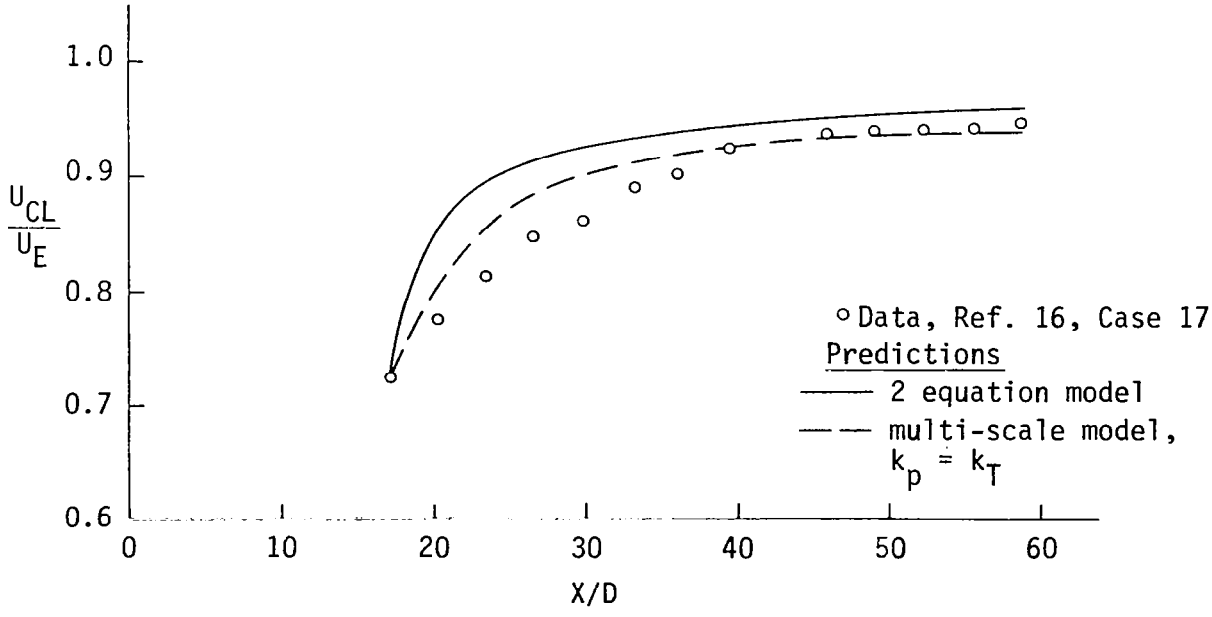

Fig. 3-14. Supersonic Axisymmetric Wake

3.4 SHEAR LAYERS

The two-dimensional shear layer is a mixing region that forms between two uniform, but different velocity streams. Although difficult to generate, it is an important laboratory flowfield; moreover, the behavior of shear layers is fundamental to the initial region of jets, and to flow over cavities and steps. It is thus an important component of an overall scramjet combustor flowfield.

Two aspects of shear layer development have been considered in this study. These are the effect of velocity ratio on shear layer growth rate, for incompressible shear layers, and the effect of Mach number on shear layer growth rate, for compressible shear layers. In both cases, the shear layer growth rate parameter has been defined in the manner called for in the 1972 Langley Symposium (Ref. 16):

$$\sigma = 1.855\ (x_2-x_1)/(y_2-y_1)$$

where y_1 and y_2 are the distances between the points at which $(U-U_E)/(U_I-U_E)$ is 0.1 and 0.9 at stations x_1 and x_2.

Since σ is determined in the fully-developed shear layer region, initial conditions for shear layer computations are unimportant. For these calculations, the initial velocity profiles reported by Lee (Ref. 16, Test Case 4) were used along with Maise and McDonald (Ref. 20) eddy viscosity profiles; for velocity and Mach number ratios other than that studied by Lee, the experimental profiles were appropriately scaled. In all cases, the strong-shear kinetic energy partition was used.

Figure 3-15 shows the fully-developed incompressible shear layer velocity profile computed for a velocity ratio of 0.375, compared to the data obtained by Spencer (Ref. 32) and by Brown and Roshko (Ref. 33). It should be noted that in computing this profile, the viscosity has been assumed to be constant at the profile edges: that is, for $(U-U_E)/(U_I-U_E) < 0.1$, the viscosity is equal to the value at $(U-U_E)/(U_I-U_E) = 0.1$, and the viscosity is also held constant for $(U-U_E)/(U_I-U_E) \geq 0.90$. This modification is often made to improve profile edge predictions.

Results for the change in shear layer growth parameter with velocity ratio are shown in Figure 3-16, compared to the empirically derived correlation,

$$\frac{\sigma_0}{\sigma} = \frac{1 - U_E/U_I}{1 + U_E/U_I}$$

which has been found to fit most incompressible shear layer data. The agreement with this correlation obtained using the multiple-scale model is excellent.

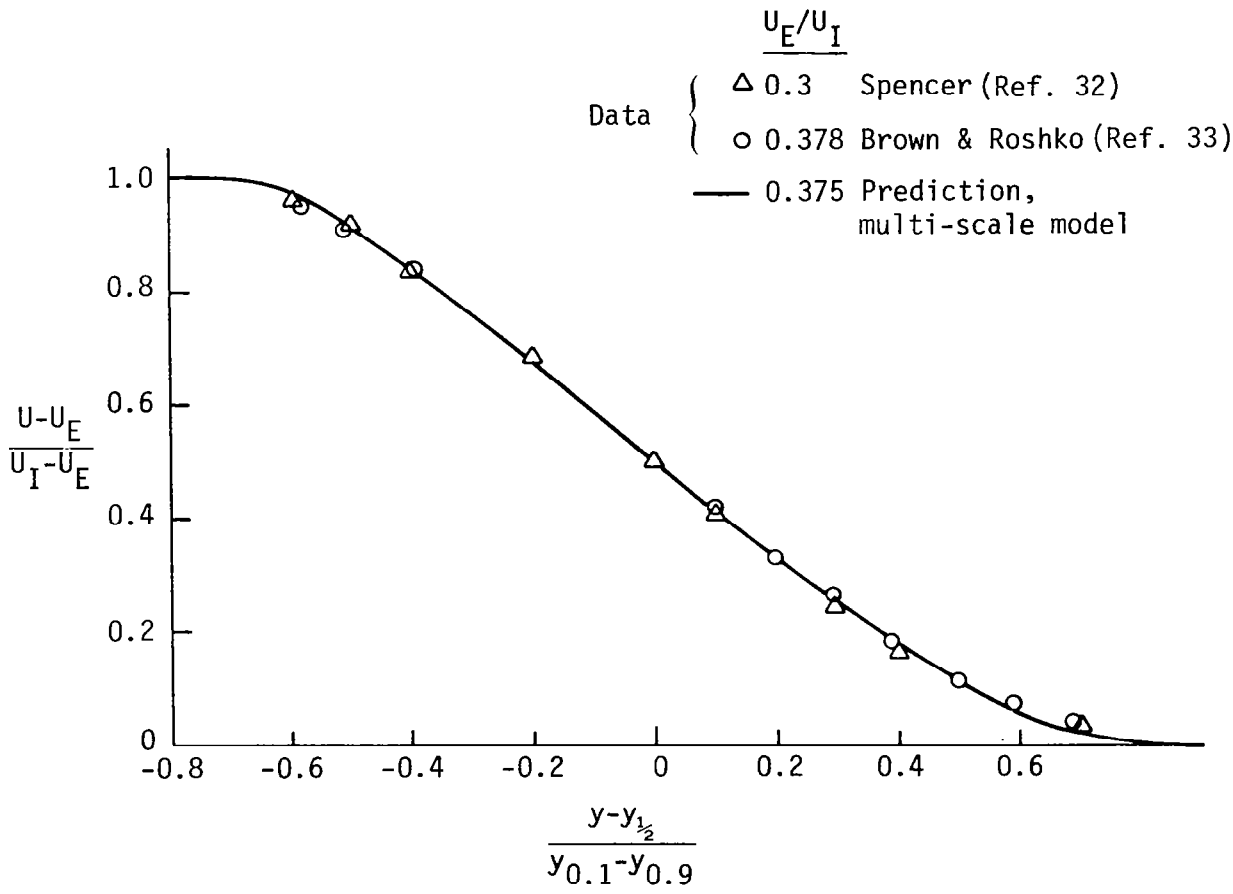

Fig. 3-15. Comparison of Predicted Fully-Developed Shear Layer Velocity Profile With Experimental Data

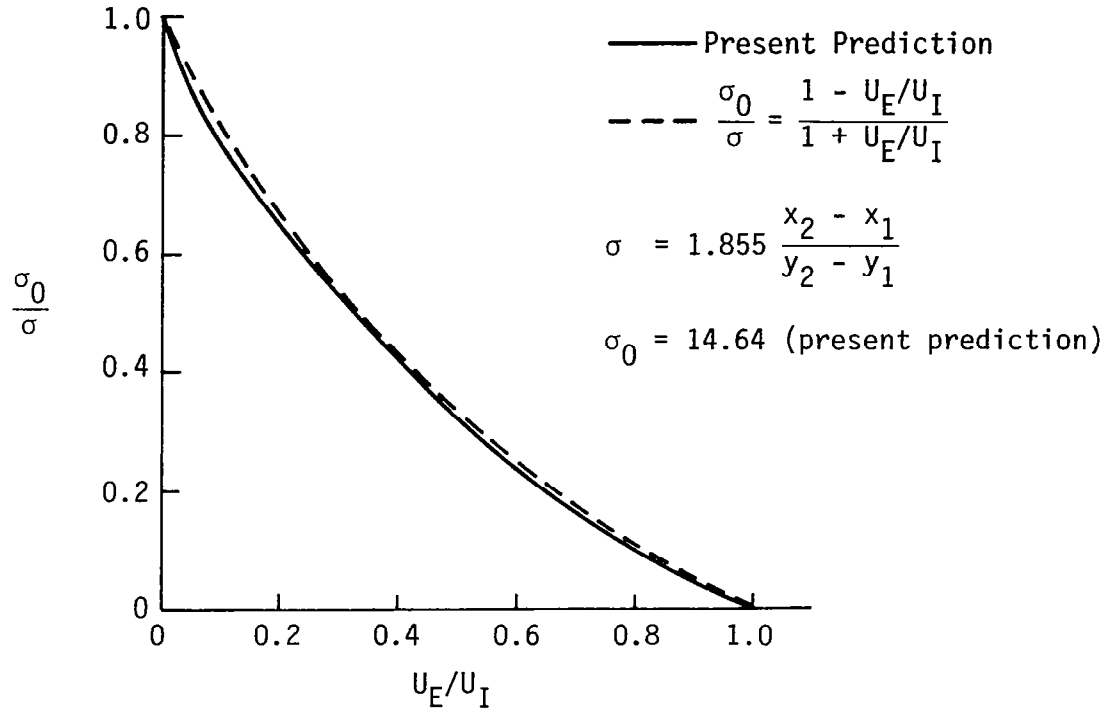

Fig. 3-16. Two-Dimensional Mixing Layer, Far Field Test, Low Mach Number

Computations of shear layer growth rate parameter, σ, as a function of high-speed stream Mach number are shown in Figure 3-17. Both recent shear layer data and supersonic jet potential core length data indicate that as Mach number increases, the growth parameter σ also increases markedly. The parameter σ is inversely proportional to the rate of increase of shear layer width; thus as Mach number increases, shear layers are observed to grow more slowly. This results in an increase in jet potential core length observed for supersonic jet flow, as already noted. However, the basic multiple-scale model predicts a small increase in σ with high-speed stream Mach number increase, which is consistent with the underprediction of high-speed jet potential core length also observed with this turbulence model.

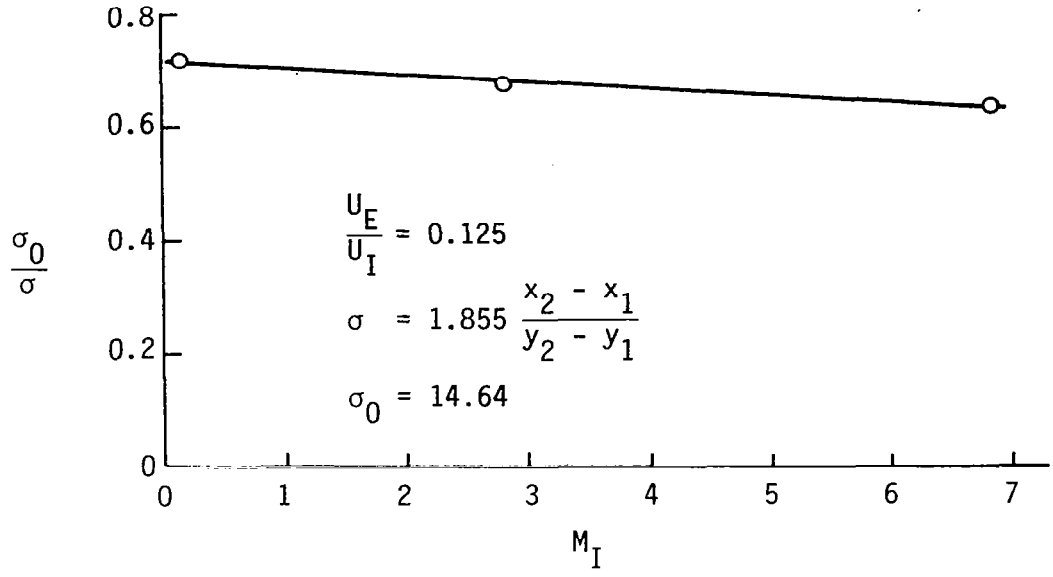

Fig. 3-17. Predicted Effect of Mach Number on Shear Layer Growth Rate

3.5 TWO-GAS FLOWS

An area of direct interest in scramjet combustor modeling is the mixing of dissimilar gases. Many scramjet concepts involve the injection of gaseous hydrogen fuel into supersonic airstreams, so that investigation of the performance of turbulence models has direct application to the use of advanced turbulence models in scramjet combustor analyses. These flowfields introduce strong density variations, particularly for hydrogen-air flows, as well as the problem of species transport. For the latter problem, species diffusion is usually modeled using the same turbulent viscosity as for momentum, modified by a Schmidt number which is generally in the range 0.7-1.0. (Since for most turbulent mixing problems, the Lewis number is unity, and the Lewis number is the ratio of the Prandtl and Schmidt numbers, the turbulent Prandtl number is usually used for both energy and species diffusion.) However, while for convenience the Prandtl (and Schmidt) numbers are usually assumed uniform throughout the flow, there is some evidence that they are actually variable. For the calculations discussed here, uniform Prandtl and Schmidt numbers have been assumed.

A well-documented study of hydrogen-air mixing phenomena is that carried out by Chriss (Refs. 34, 35) and used as test case 10 of Ref. 16. The apparatus used to generate the flowfield consisted of an 8.89 cm (3.5 inch) subsonic air nozzle which formed an annulus around an inner subsonic hydrogen nozzle. The inner nozzle had an exit inside diameter of 1.27 cm (0.5 in.) and a nozzle lip thickness of 0.127 mm (0.005 in.). For the case considered, the hydrogen stream velocity was 1006 m/sec (3300 ft/sec) and the hydrogen stream/air stream velocity ratio (U_E/U_j) was 6.30. Initial conditions were defined at the initial measurement station, X/D = 2.966, using measured mean velocity profiles and constant eddy viscosity values chosen to reproduce the shear stress data contained in Ref. 34.

Results of the computations carried out for this case are shown in Figure 3-18. In all cases, the basic two-equation model and the multiple-scale model with either $k_p = k_T$ or $k_p = 4k_T$, the velocity potential core length is overpredicted, as is the concentration potential core length. A constant turbulent Prandtl number value of 0.85 was used in all calculations, as noted in Figure 3-18. These results may indicate the necessity for a density ratio modification to the turbulence model; however, as the rate of decay of both velocity and concentration is predicted reasonably well in all the calculations shown, it is not clear from this comparison alone that such a correction is, in general, necessary.

The details of the velocity and concentration profiles are reasonably well predicted for this flowfield, as shown in Figures 3-19 and 3-20. Note that these profiles are normalized with local centerline values, and thus do not reflect the spatial mismatch apparent in Figure 3-18.

A second hydrogen-air mixing case considered in this study involves the data obtained by Eggers, Ref. 36, and used as test case 22 of Ref. 18. In this case, a subsonic hydrogen stream is surrounded by a supersonic air stream. The outer air nozzle was designed for a Mach number of 2.50 and had an exit diameter of 15.2 cm (6.0 in.); the inner nozzle, 1.16 cm (0.46 in.) in diameter, was designed to produce a Mach number 0.91 hydrogen flow. The jets mixed in an unconfined region at a static pressure of one atmosphere.

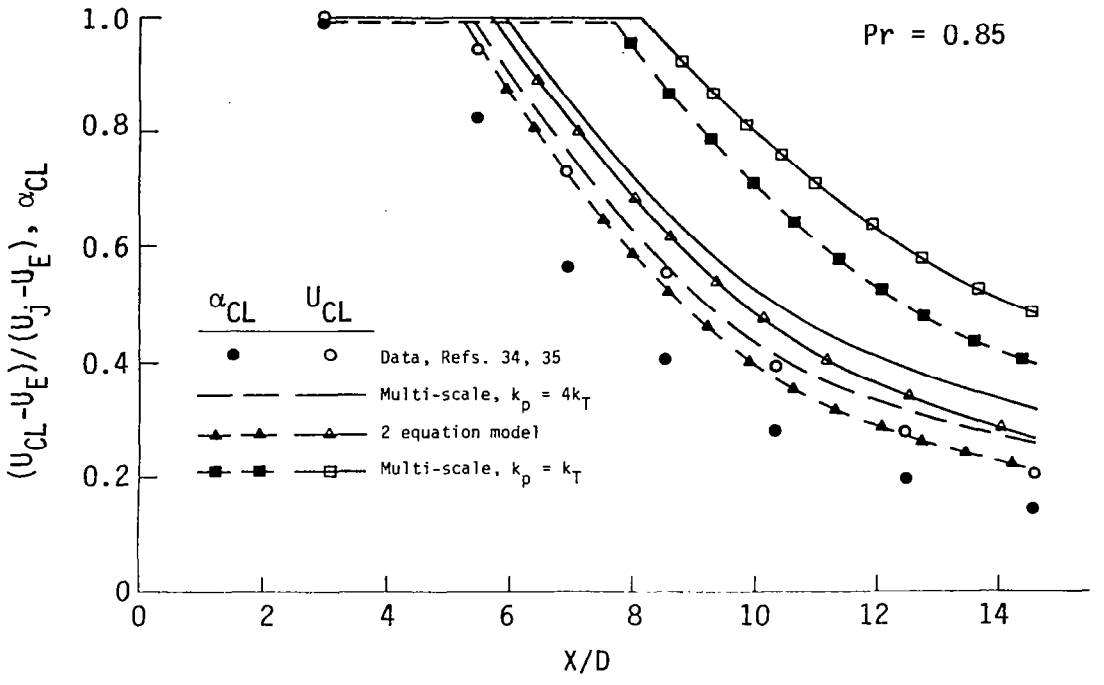

Fig. 3-18. Coaxial Hydrogen Air Jets

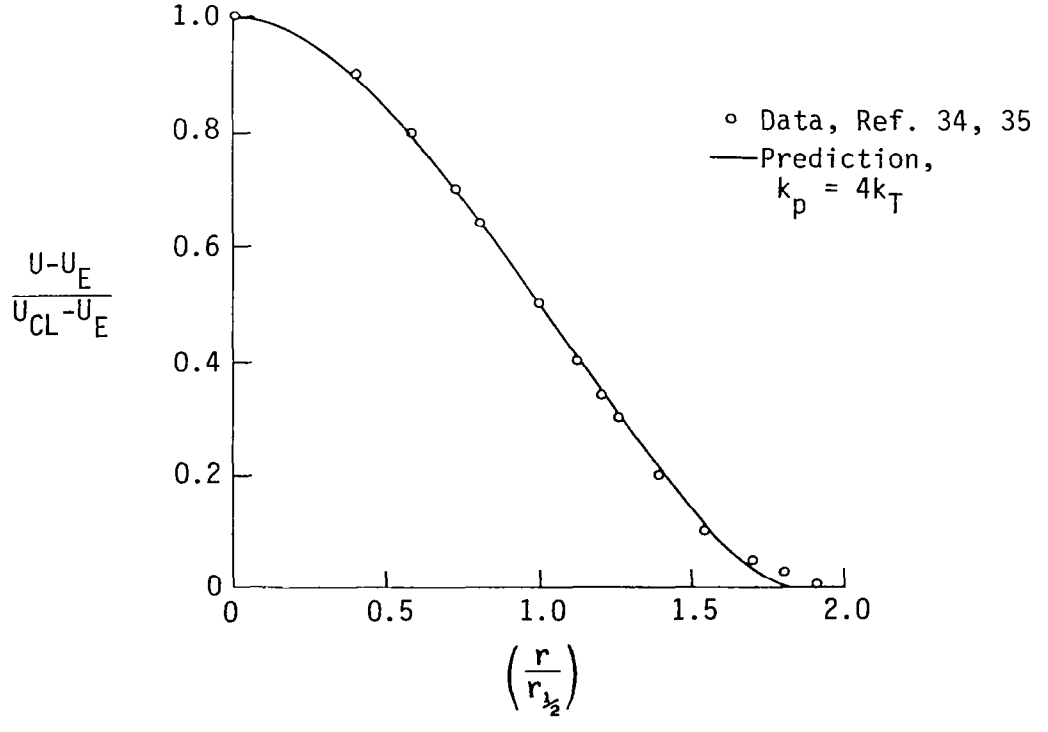

Fig. 3-19. Velocity Profiles, Axisymmetric Hydrogen in Air Jets at X/D = 14. Half-radius based on local velocity profile.

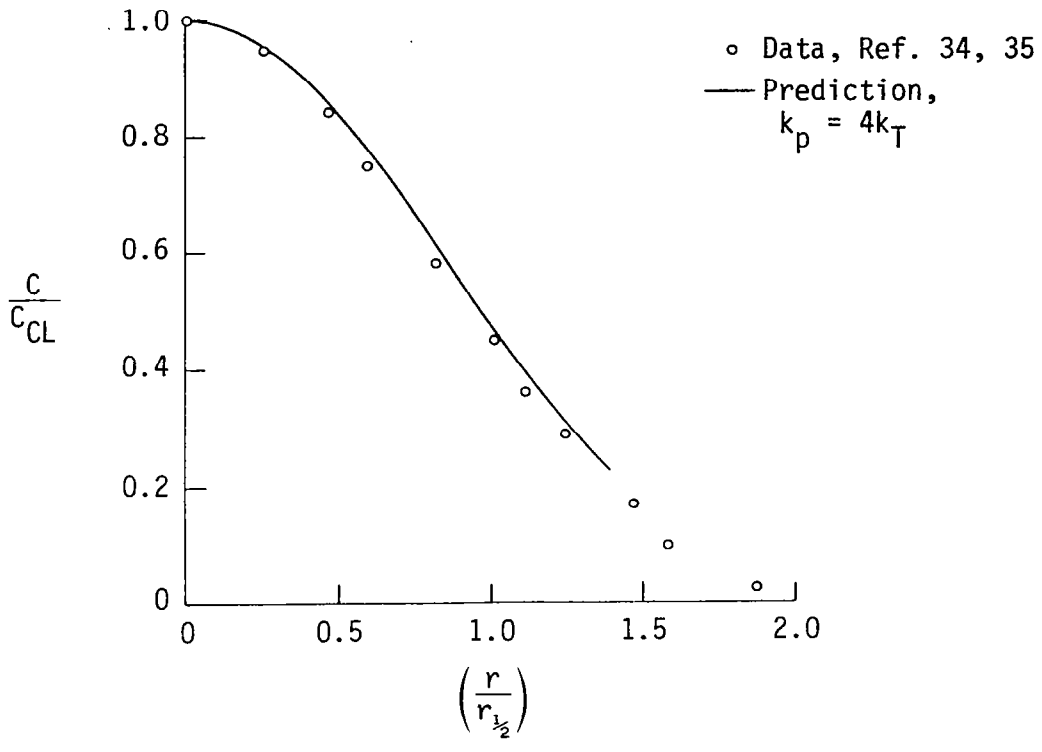

Fig. 3-20. Concentration Profiles, Axisymmetric Coaxial Hydrogen in Air Jets at X/D = 14. Half-radius based on local concentration profile.

Initial conditions for this flow were established at the nozzle exit, using measured mean velocity profiles and the Maise and McDonald (Ref. 20) eddy viscosity profiles to establish the initial turbulent kinetic energy levels. The strong-shear partition assumption, $k_p = 4k_T$ was used as part of the initial conditions for this calculation. Results of the multiple-scale model computation of this flowfield are shown in Figure 3-21, which indicates that the basic multiple-scale model provides a reasonably good representation of this flow. Noteworthy is the decrease in centerline velocity below that on the edge of the flow for X/D > 18 shown by both the data and the computations. This behavior is caused by the fact that from a momentum flux standpoint this flowfield is wakelike in character: despite the relatively high velocity of the center jet, the density of the jet flow is so low that its momentum flux is substantially less than that of the outer stream.

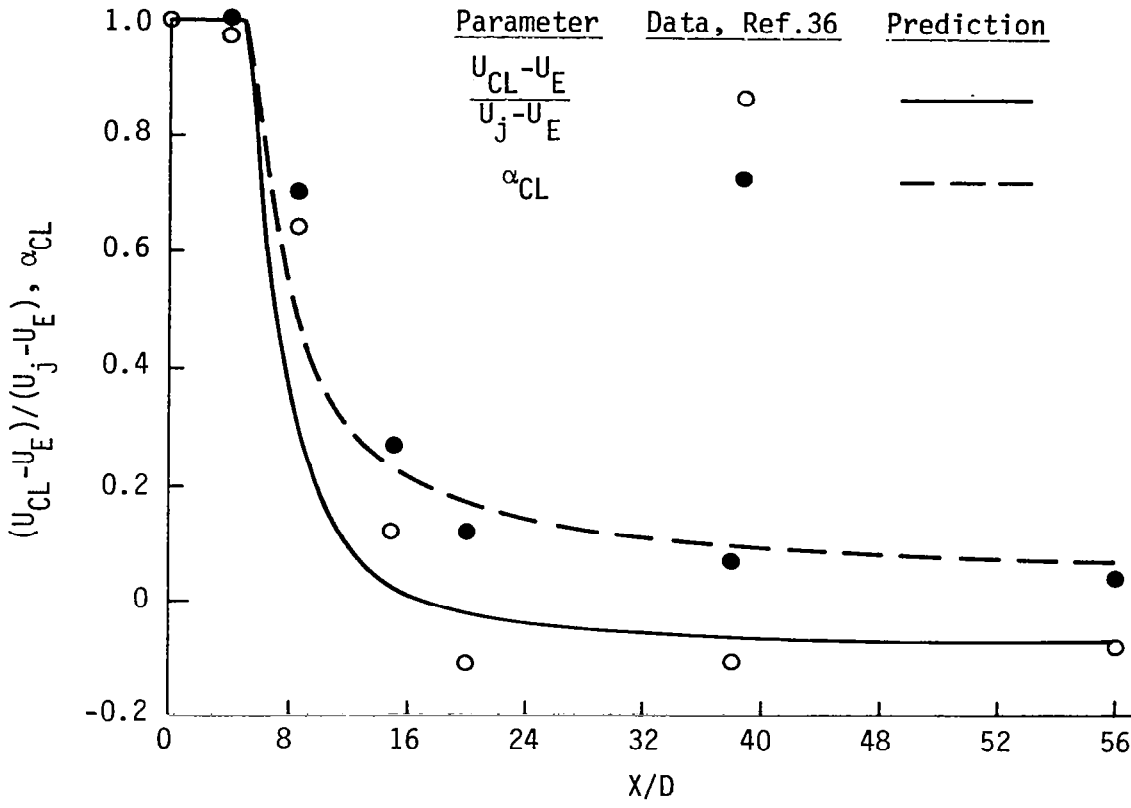

Fig. 3-21. Compressible Coaxial Hydrogen-Air Jets

3.6 COMPRESSIBILITY CORRECTION

It is evident from the comparisons so far presented that the multiple-scale model does not markedly improve the prediction of the two-equation model insofar as compressibility effects are concerned. Thus, an examination of possible compressibility correction terms was initiated. This examination centered on the modification of the irrotational strain term, which represents (albeit in a somewhat ad hoc manner) the effects of dilatation on turbulence production. The effects of compressibility can be shown from the continuity equation to involve the dilatation, or irrotational component of the strain field. The data for the supersonic jet into still air (Ref. 29), test case 7 of Ref. 16, were utilized in this preliminary assessment.

Figure 3-22 shows the results of this initial evaluation. It is clear that the coefficient C'_{p1} has a marked influence on the potential core length

for this flowfield, and that a value of -0.100 (compared to -0.110 as recommended by Launder) provides a markedly improved prediction. Since the value $C'_{p1} = -0.110$ provides good results for $M \simeq 0$, the simple correction equation $C'_{p1} = -0.110 + 0.009\ M$ was devised. As Figure 3-22 indicates, this provided a very good prediction of the flowfield development. For a sensitivity check, $C'_{p1} = -0.110 + 0.0045\ M$ was also investigated: the results of this computation fall in between the unmodified model results and those using the initially described modification.

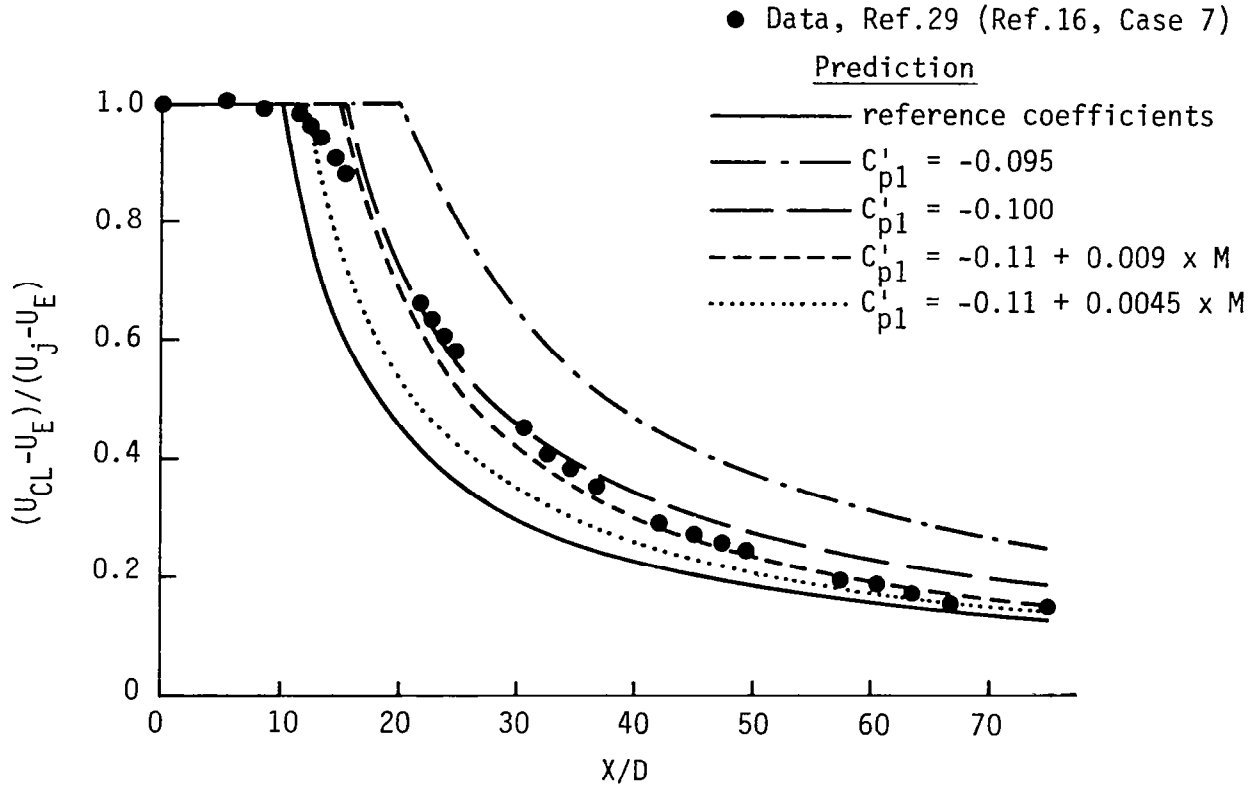

Fig. 3-22. Effect of Compressibility Corrections on Supersonic Jet Predictions

Given the results shown in Figure 3-22, the effect of this preliminary compressibility correction model on the prediction of shear layer growth rate as a function of Mach number was investigated. It will be recalled that the basic multiple-scale model predicts a very slow increase of the shear layer

growth parameter, σ, with Mach number, whereas recent shear layer data and inferential evidence from jet experiments indicate a strong increase in σ with Mach number. The results of this investigation are shown in Figure 3-23, which shows that the postulated compressibility correction has a strong influence, increasing the value of σ (and thus decreasing the effective growth rate of the shear layer) as a function of Mach number.

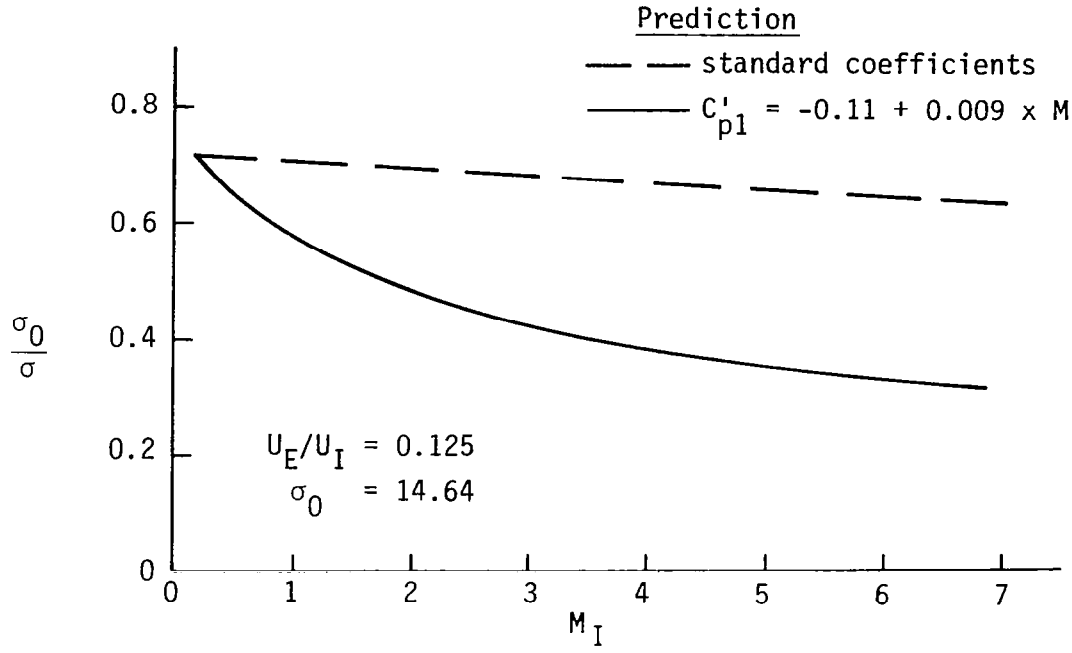

Fig. 3-23. Effect of Compressibility Correction on Shear Layer Growth Rate as a Function of Mach Number

The calculations shown in Figure 3-23 were carried out for a velocity ratio of 0.125, and thus cannot be compared directly with data obtained for $U_E/U_I = 0$; indirect comparison is also difficult since as Mach number is increased, both stream Mach numbers increase in these computations, while this is not the case when $U_E/U_I = 0$. Nevertheless, these results show an increase of σ at Mach 5 compared to $M \simeq 0$ of a factor of 2.3, while available data indicates an increase of 2.8-3.0 over the same Mach number range for $U_E/U_I = 0$ (Ref. 16).

Finally, the effect of the compressibility correction term on the supersonic air/subsonic hydrogen mixing data of Eggers (Ref. 36); case 22 of Ref.16,

was investigated. The results of these computations are shown in Figure 3-24. In this case, the compressibility correction appears to produce no significant effect on the predicted potential core length, although for this flow the potential core length is so short that the effect may not be observable. On the other hand, the initial velocity and species decay rates were markedly affected. In this computation, the use of the compressibility correction appears to improve the initial decay rate prediction, at the expense of the prediction of the later period of decay.

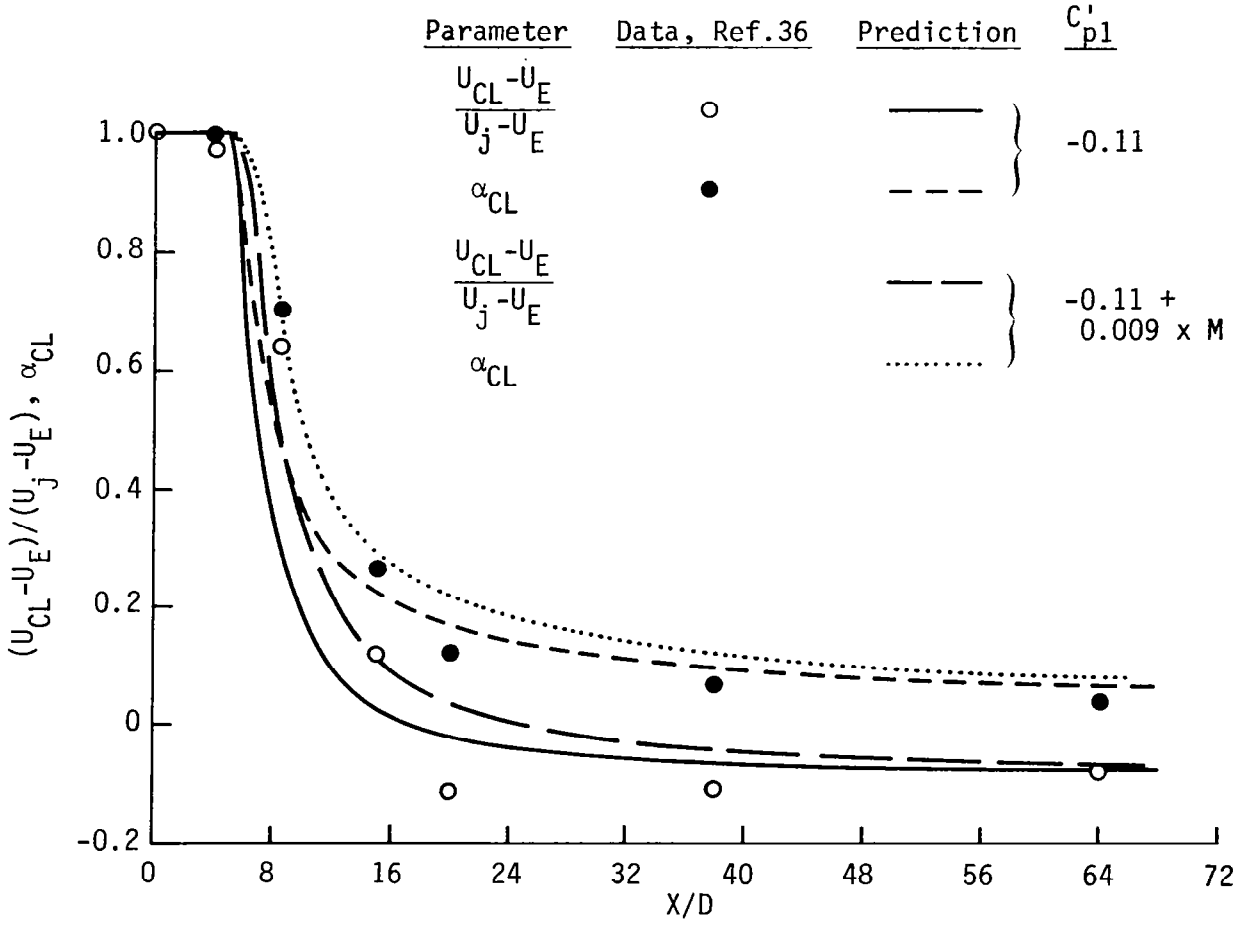

Fig. 3-24. Effect of Compressibility Correction, H_2/Air Mixing

3.7 INCOMPRESSIBLE ELLIPTIC FLOWS

All of the results so far discussed have been obtained for parabolic, boundary-layer type flowfields. For these flows, a variety of reasonably exact numerical solution techniques exist with which to integrate the equations of motion, and numerical solution difficulties do not usually interfere with turbulence model evaluation. Such is, unfortunately, not the case for elliptic flowfields. For these flows, which involve recirculation regions, techniques for the solution of the full Navier-Stokes equations of motion are required. While a variety of such techniques exist, none is completely free from numerical difficulties that can complicate the investigation of turbulence models.

As part of the current program, investigation of the application of turbulence models to the prediction of incompressible recirculating flows has been initiated. The investigation involves the use of an implicit finite-difference solution of the Navier-Stokes equations that is similar to the Imperial College TEACH code. While this code is flexible and general in its formulation, an adequate solution for the purposes of turbulence model investigation requires great care and considerable computer resources.

The flowfield under consideration in this investigation is the incompressible, sudden-expansion flow described by Chaturvedi (Ref. 37). This flowfield involves an area ratio of 4, and the inlet turbulent intensity was extremely low, of the order of $10^{-4}U_j^2$. Computations were carried out using the basic two-equation turbulence model, with the initial turbulence intensity set at the value indicated by the data, and also at the value of $0.01U_j^2$ generally recommended for use with the code. The corresponding dissipation values were set equal to $C_D k^{1.5}/\ell_{max}$, where ℓ_{max} is proportional to the distance from the wall and $C_D = 0.09$. At the exit plane, the static pressure is assumed uniform and constant and the axial gradients of all dependent variables vanish. Wall boundary conditions for k and ε are evaluated by assuming that a local equilibrium exists between production and dissipation of turbulent kinetic energy, and that the length scale varies linearly with distance from the wall. Using this approach, the wall region turbulent kinetic energy and dissipation rate are, respectively:

$$k_p = \tau_w/\rho_w C_D^{\frac{1}{2}}$$

$$\varepsilon_p \frac{Y_p}{k_p^{3/2}} = C_D^{3/4}/\eta$$

where η, Von Karmans's constant, is taken to be 0.4.

Computations were carried out using several grid sizes. The initial calculations used a 13 (radial) x 25 (axial) grid, and provided surprisingly good agreement with the experimental data, except near the wall. However, despite achieving a reasonably good level of convergence based on the mass imbalance criterion embodied in the code, the predicted recirculation zone length was about half of that experimentally measured. To improve the near-wall region, and thus the recirculation zone prediction, finer grid spacings were tried. The first of these, a 50 (radial) x 50 (axial) grid did not produce useful results because of excessive grid aspect ratio ($\Delta x/\Delta r$). The second, 25 (radial) x 100 (axial) provided very good results.

Figures 3-25 through 3-30 depict the radial profiles of axial velocity and turbulent kinetic energy predicted using the two-equation turbulence model compared to the data obtained by Chaturvedi. With a 25 x 100 grid and 1000 iterations, very good results have been obtained for the mean velocity profiles (although the mean velocity profiles obtained using a 13 x 25 grid were within 10% of these values). The kinetic energy levels in the shear layer region bounding the recirculation zone are strongly overpredicted (Figures 3-27 and 3-28), but downstream of the recirculation zone the kinetic energy levels rapidly relax to the measured values.

Centerline velocity and kinetic energy values obtained using the basic two-equation model are shown in Figure 3-31 in comparison with the experimental data. Clearly, the prediction obtained with the experimental initial turbulence levels (as used in the comparisons previously discussed) is superior to that obtained with an arbitrary, $k_I = 0.01U_j^2$ initial condition. The initial rate of increase of the kinetic energy is, however, underpredicted for this flow: this may reflect transition mechanisms that are not incorporated in the model.

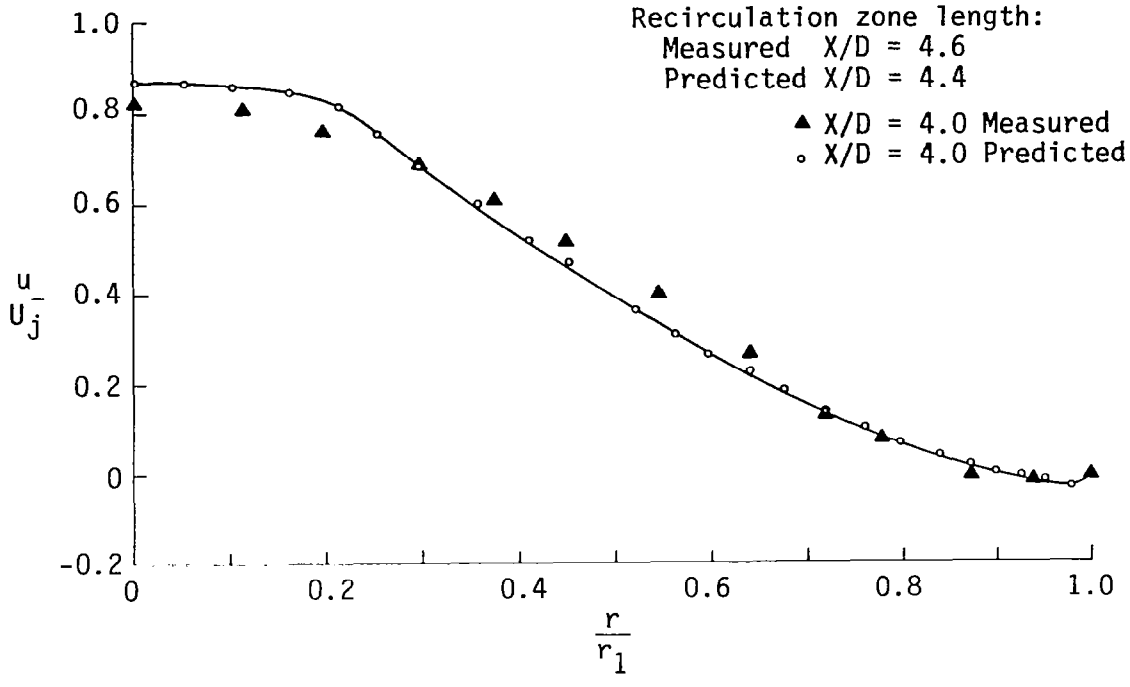

Fig. 3-25. Axial Velocity Profile - Chaturvedi Data (Ref. 37)

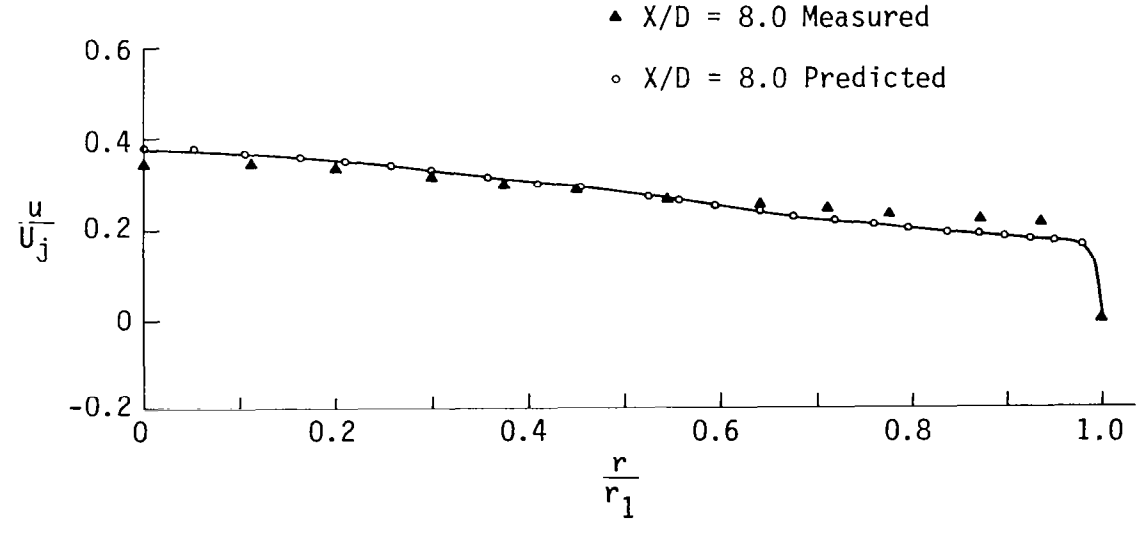

Fig. 3-26. Axial Velocity Profile - Chaturvedi Data (Ref. 37)

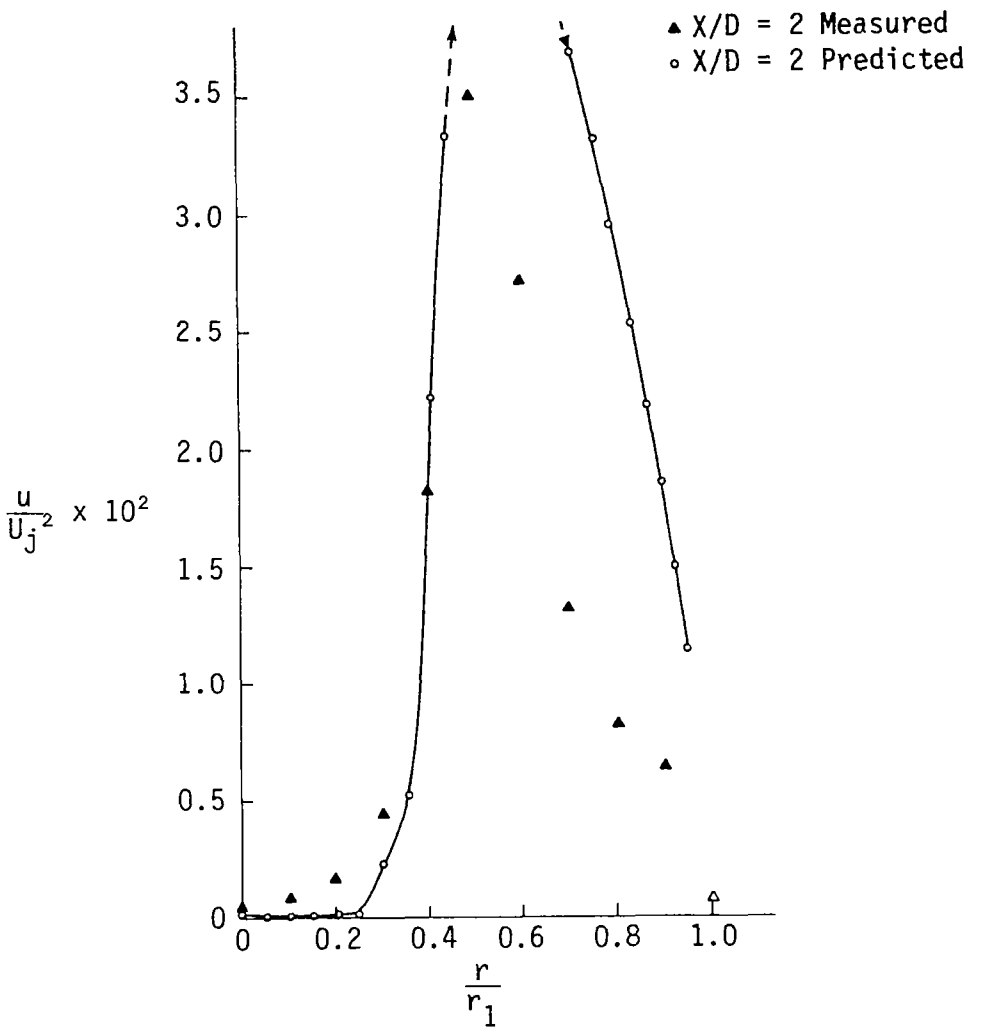

Fig. 3-27. Radial Turbulent Kinetic Energy Profile, Chaturvedi Data (Ref. 37)

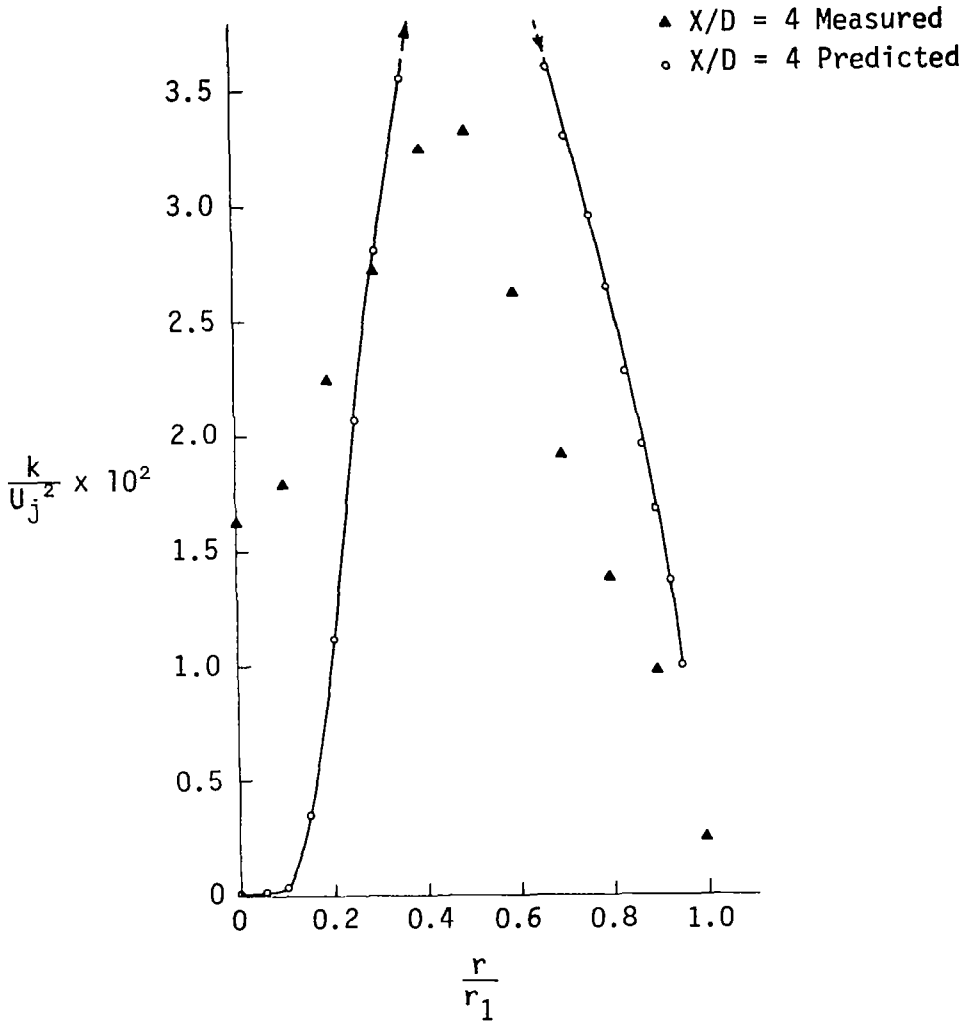

Fig. 3-28. Radial Turbulent Kinetic Energy Profile, Chaturvedi Data (Ref. 37)

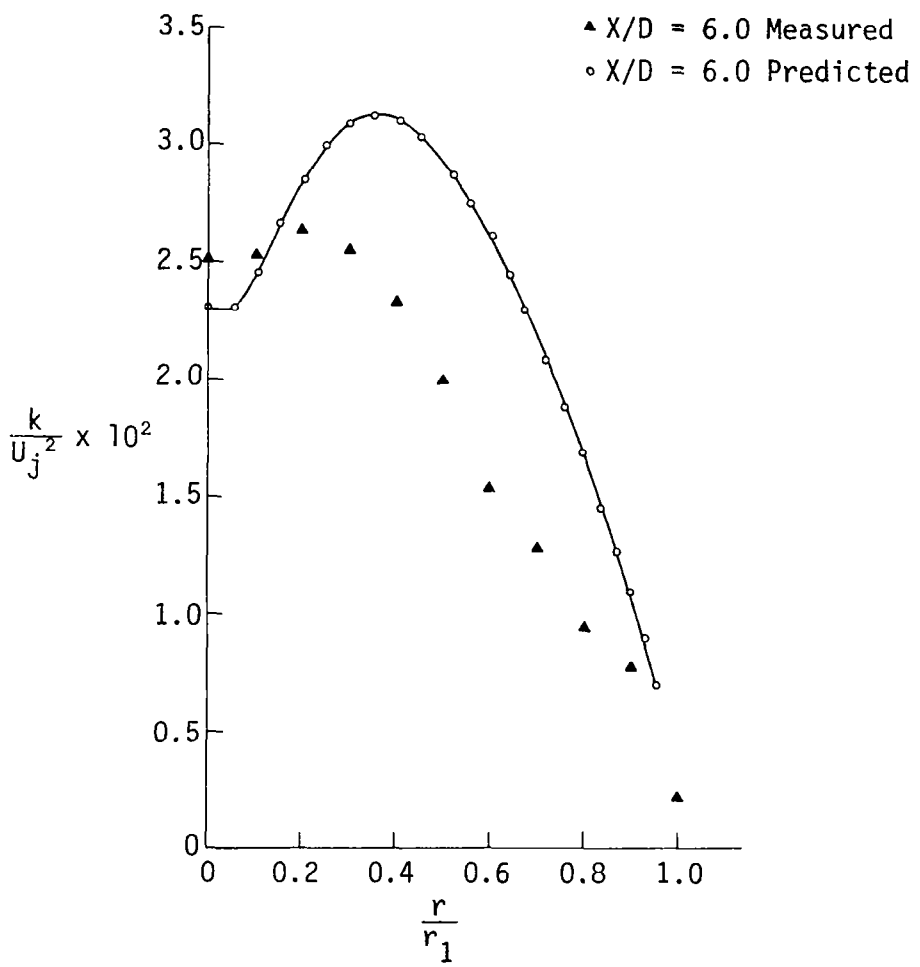

Fig. 3-29. Radial Turbulent Kinetic Energy Profile, Chaturvedi Data (Ref. 37)

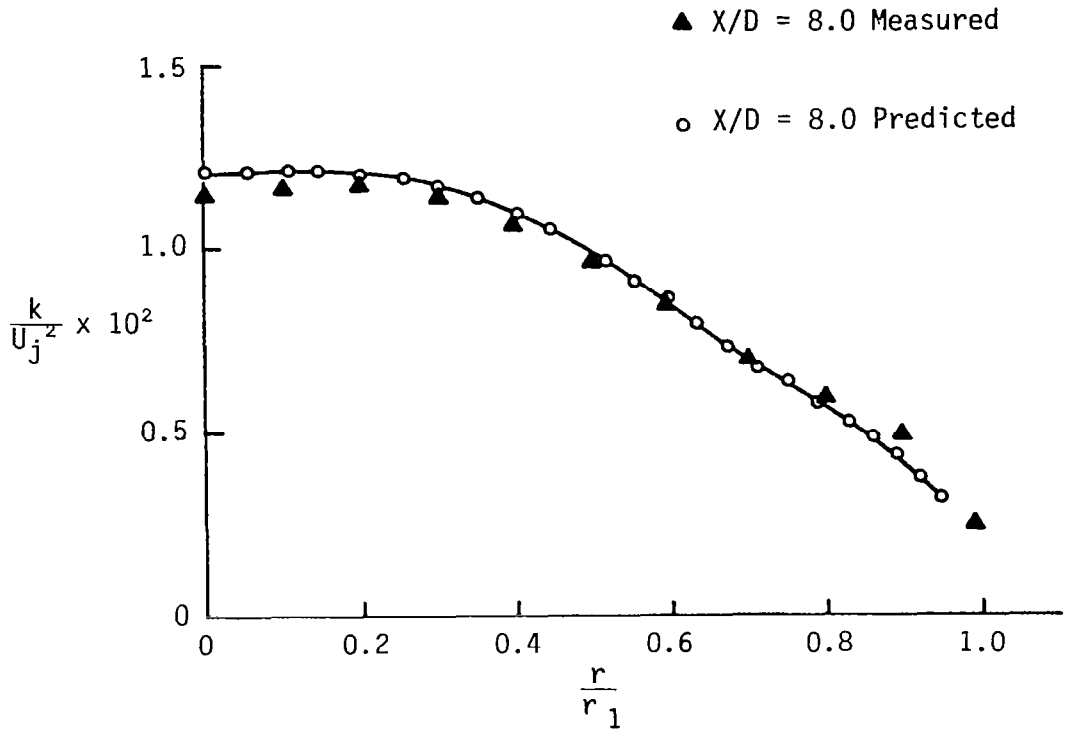

Fig. 3-30. Turbulent Kinetic Energy Profile, Chaturvedi Data (Ref. 37)

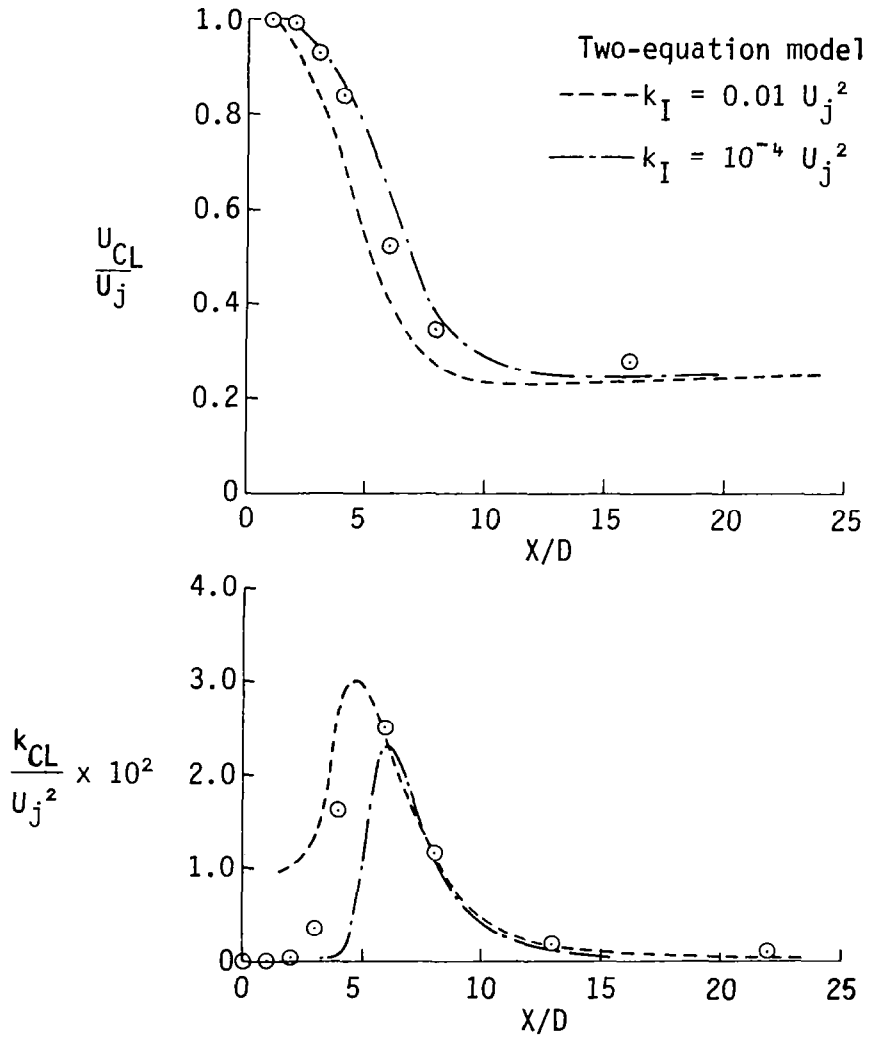

Fig. 3-31. Centerline Velocity and Turbulent Kinetic Energy Profiles, Chaturvedi Data (Ref. 37)

4. CONCLUSIONS AND RECOMMENDATIONS

Before a turbulence model can be considered to be reliable, it must be thoroughly tested. This statement risks status as a tautology, yet it must be taken seriously in the context of the application of turbulence models to the engineering prediction of flowfields. One result of this study has been to thoroughly test the application of the multiple-scale turbulence model to a variety of flows of interest in scramjet combustor applications. Because most of the available data are for boundary-layer type flows, and because the numerical solution of these flowfields introduces little inaccuracy and complexity, this study has focused primarily on free jet and wake flowfields. Unfortunately, this emphasis has tended to mask some of the more important attributes of the multiple-scale model. For example, Hanjalic, Launder, and Schiestel (Ref. 5) have shown that the multiple-scale model provides greatly improved prediction of the development of a boundary layer in a strong adverse pressure gradient; this flowfield was not considered in the present study.

The bulk of the flowfields considered in this work have been those documented in the 1972 NASA-Langley Symposium on Free Turbulent Shear Flows. These flowfields have been emphasized because they are well-documented and include a wide variety of important phenomena, including the effects of compressibility and of density gradients caused by molecular weight variation. Further, the use of these data allows comparison of the predictions of the multiple-scale model with those of other turbulence models.

In general, this investigation has shown that the multiple-scale model provides a reliable prediction of the free shear flows included in the 1972 Symposium. It has also been shown that, despite the increased complexity of the multiple-scale approach in comparison with some other turbulence models, it is possible to achieve reliable results using a standardized technique for estimation of initial conditions where detailed initial data do not exist.

The application of a simple compressibility correction technique to improve the predictions of the basic incompressible multiple-scale approach in supersonic flows has also been demonstrated.

The present study has shown that the multiple-scale model is capable of increasing the generality of the basic two-equation model without seriously compromising any of the capabilities inherent in the two-equation formulation. Thus, it can be confidently applied to the prediction of more complex flows, where its particular advantages should be more apparent. This study has also again highlighted the difficulty of investigating turbulence modeling in more complex flows which require more sophisticated numerical solution techniques than parabolic, boundary layer flows. This conclusion is not unique: Pope and Whitelaw (Ref. 13) have also remarked on the difficulties involved in assessing turbulence models in complex flows, although their focus was more on the problems of initial and boundary condition specification than numerical difficulties per se.

Further development of turbulence models for scramjet applications should focus on several specific areas:

1. Both the two-equation model and the multiple-scale model require corrections for compressibility and, possibly, density ratio effects. The improvements to be gained through the development of compressibility corrections to the multiple-scale model have been indicated by the work described in this report. This area of research should continue.

2. The multiple-scale model should be applied to the prediction of more complex flows, specifically subsonic and supersonic boundary layers undergoing strong pressure gradients.

3. Both the algebraic Reynolds stress formulation and the use of the multiple-scale model should be investigated for application to two-dimensional recirculating and three-dimensional parabolic flows. It should, however, be recognized that in these areas the development of numerical techniques is the pacing criterion.

5. REFERENCES

1. Drummond, J. P.; Rogers, R. C.; and Evans, J. S.: Combustor Modelling for Scramjet Engines. AGARD Conference Proceedings No. 275, Combustor Modelling, February 1980, Paper 10.
2. Schetz, Joseph A.: Injection and Mixing in Turbulent Flow. Progress in Astronautics and Aeronautics, vol. 68, AIAA, 1980.
3. Launder, B. E.; and Schiestel, R.: On the Utilization of Multiple Time Scales in the Modeling of Turbulent Flow. C. R. Acad. Sc. Paris, vol. 286, Series A, 24 April 1978, pp. 709-712 (in French).
4. Launder, B. E.; and Schiestel, R.: Application of a Multiple Scale Turbulence Model to the Calculation of Free Shear Flows. Submitted to C. R. Acad. Sci. Paris (in French).
5. Hanjalić, K.; Launder, B. E.; and Schiestel, R.: Multiple-Time-Scale Concepts in Turbulent Transport Modeling. Paper presented at Second Symposium on Turbulent Shear Flows, July 2-4, 1979, Imperial College, London.
6. Rodi, W.: The Prediction of Free Turbulent Boundary Layers by Use of a Two-Equation Model of Turbulence. Ph.D. Thesis, Univ. of London, 1972.
7. Bray, K. N. C.: Equations of Turbulent Combustion. I Fundamental Equations of Reacting Turbulent Flow. AASU Report No. 330, Univ. of Southampton, Department of Aeronautics and Astronautics, Southampton (England), October 1973.
8. Favre, A. J.: The Equations of Compressible Turbulent Gases. Summary Report No. 1, Contract AF 61(052)-772, Institute de Mecanique Statistique de la Turbulence, Univ. d' Aix-Marseille, January 1965 (AD 622079).
9. Bradshaw, P.; Cebeci, T.; and Whitelaw, J. H.: Lecture Series on Engineering Calculation Methods of Turbulent Flows. Mechanical Engineering Department, California State University Long Beach, 20-23 June 1977.

10. Stanford, R. A.; and Libby, P. A.: Further Applications of Hot-Wire Anemometry to Turbulence Measurements in Helium-Air Mixtures. Phys. Fluids, vol. 17, no. 7, July 1974, pp. 1353-1361.

11. Launder, B. E.; Morse, A.; Rodi, W.; and Spalding, D. B.: Prediction of Free Shear Flows - A Comparison of the Performance of Six Turbulence Models. Free Turbulent Shear Flows, vol. 1, Conference Proceedings, NASA SP-321, 1973, pp. 361-426.

12. Launder, B. E.; and Spalding, D. B.: Mathematical Models of Turbulence, Academic Press, 1972.

13. Pope, S. B.; and Whitelaw, J. H.: The Calculation of Near-Wake Flows. J. Fluid Mech., vol. 73, part 1, pp. 9-32, 1976.

14. Hanjalić, K.; and Launder, B. E.: Sensitizing the Dissipation Equation to Irrotational Strains. J. Fluids Engineering, Trans. ASME, vol. 102, March 1980, pp. 34-40.

15. Peters, C. E., and Phares, W. J.: An Integral Turbulent Kinetic Energy Analysis of Free Shear Flows. Free Turbulent Shear Flows, Vol. I, Conference Proceedings, NASA SP-321, 1973, pp. 577-628.

16. Free Turbulent Shear Flows. Vol. 1, Conference Proceedings, vol. 2, Summary of Data. NASA SP-321, 1973.

17. Boccio, J. L.; Weilerstein, G.; and Edelman, R. B.: A Mathematical Model for Jet Engine Combustor Pollutant Emissions. NASA CR-121208, March 1973.

18. Gosman, A. D.; and Pun, W. M.: Lecture Notes for a Course Entitled 'Calculation of Recirculating Flows.' Imperial College of Science and Technology, Mechanical Engineering Department, Report HTS/74/2, December 1973.

19. Harsha, P. T.: A General Analysis of Free Turbulent Mixing. AEDC TR 73-177, Arnold Engineering Development Center, Arnold Air Force Station, Tennessee, May 1974 (AD 778415).

20. Maise, G.; and McDonald, H.: Mixing Length and Kinetic Eddy Viscosity in a Compressible Boundary Layer. AIAA J., vol. 6, no. 1, January 1978, pp. 73-80.

21. Harsha, P. T.; and Lee, S. C.: Correlation Between Turbulent Shear Stress and Turbulent Kinetic Energy. AIAA J., vol. 8, 1970, pp. 1508-1510.

22. Wygnanski, I.; and Fiedler, H.: Some Measurements in the Self-Preserving Jet. J. Fluid Mech., vol. 38, part 3, September 18, 1969, pp. 577-612.
23. Bradshaw, P.; Ferriss, D. H.; and Johnson, R. F.: Turbulence in the Noise-Producing Region of a Circular Jet. J. Fluid Mech., vol. 19, part 4, August 1964, pp. 591-624.
24. Harsha, P. T.: Free Turbulent Mixing: A Critical Evaluation of Theory and Experiment. AEDC-TR-71-36, Arnold Engineering Development Center, February 1971.
25. Rodi, W.: A Review of Experimental Data of Uniform Density Free Turbulent Boundary Layers. Studies in Convection, vol. 1, B. E. Launder, ed. Academic Press, 1975, pp. 79-166.
26. Albertson, M. L.; Dai, Y. B.; Jensen, R. A.; and Rouse, H.: Diffusion of Submerged Jets. Transactions ASCE, vol. 115, 1950, pp. 643-664.
27. Baines, W. D.: Diffusion of Submerged Jets-Discussion. Proceedings ASCE, vol. 75, no. 7, September 1949, pp. 1019-29.
28. Maestrello, L.; and McDaid, E.: Acoustic Characteristics of a High-Subsonic Jet. AIAA J., vol. 9, no. 6, June 1971, pp. 1058-1066.
29. Eggers, James M.: Velocity Profiles and Eddy Viscosity Distributions Downstream of a Mach 2.22 Nozzle Exhausting to Quiescent Air. NASA TN D-3601, 1966.
30. Forstall, W., Jr.; and Shapiro, A. H.: Momentum and Mass Transfer in Coaxial Gas Jets. Journal of Applied Mechanics, vol. 17, December 1950, pp. 399-408. Discussion: Journal of Applied Mechanics, vol. 18, June 1951, pp. 219-220.
31. Chevray, R.: The Turbulent Wake of a Body of Revolution. Journal of Basic Engineering, Trans. ASME, vol 90, series D, no. 2, June 1968, pp. 275-284.
32. Spencer, B. W.: Statistical Investigation of Turbulent Velocity and Pressure Fields in a Two-Stream Mixing Layer. Ph.D. Thesis, Univ. of Illinois, 1970.
33. Brown, G.; and Roshko, A.: The Effect of Density Difference on the Turbulent Mixing Layer. AGARD CP-93, January 1972.

34. Chriss, D. E.: Experimental Study of the Turbulent Mixing of Subsonic Axisymmetric Gas Streams. AEDC-TR-68-133, U. S. Air Force, August 1968. (Available from DTIC as AD 672 975.)

35. Chriss, D. E.; and Paulk, R. A.: An Experimental Investigation of Subsonic Coaxial Free Turbulent Mixing. AEDC-TR-71-236, AFOSR-72-0237TR, U. S. Air Force, Feb. 1972. (Available from DTIC as AD 737 098.)

36. Eggers, James M.: Turbulent Mixing of Coaxial Compressible Hydrogen Air Jets. NASA TN D-6487, 1971.

37. Chaturvedi, M. C.: Flow Characteristics of Axisymmetric Expansion. Journal of the Hydraulics Division, Proc. ASCE, vol. 89, no. HY3, May 1963, pp. 61-92.

1. Report No.	2. Government Accession No.	3. Recipient's Catalog No.
NASA CR-3433		

4. Title and Subtitle	5. Report Date
MULTIPLE-SCALE TURBULENCE MODELING OF BOUNDARY LAYER FLOWS FOR SCRAMJET APPLICATIONS	May 1981
	6. Performing Organization Code
7. Author(s)	8. Performing Organization Report No.
G. Fabris, P. T. Harsha and R. B. Edelman	SAI-80-022-CP
	10. Work Unit No.
9. Performing Organization Name and Address	
Science Applications, Inc. Combustion Science and Advanced Technology Department 21133 Victory Boulevard, Suite 216 Canoga Park, California 91303	11. Contract or Grant No. NAS1-15988
	13. Type of Report and Period Covered
12. Sponsoring Agency Name and Address	Contractor Report
National Aeronautics and Space Administration Washington, DC 20546	14. Sponsoring Agency Code

15. Supplementary Notes

Langley Technical Monitor: John Evans
Topical Report

16. Abstract

As part of an investigation into the application of turbulence models to the computation of flows in advanced scramjet combustors, the multiple-scale turbulence model has been applied to a variety of flowfield predictions. The model appears to have a potential for improved predictions in a variety of areas relevant to combustor problems. This potential exists because of the partition of the turbulence energy spectrum that is the major feature of the model and which allows the turbulence energy dissipation rate to be out of phase with turbulent energy production. To establish the general reliability of the approach, it has been tested through comparison of predictions with experimental data from the Free Turbulent Shear Flow Conference held at NASA-Langley in 1972. The computations have been made using a consistent method of generating experimentally unavailable initial conditions. An appreciable overall improvement in the generality of the predictions is observed, as compared to those of the basic two-equation turbulence model. A Mach number-related correction is found to be necessary to satisfactorily predict the spreading rate of the supersonic jet and mixing layer.

17. Key Words (Suggested by Author(s))	18. Distribution Statement
Turbulence modeling Shear flow turbulence Turbulent mixing Compressibility effects	Unclassified - Unlimited Subject Category 34

19. Security Classif. (of this report)	20. Security Classif. (of this page)	21. No. of Pages	22. Price
Unclassified	Unclassified	72	A04

For sale by the National Technical Information Service, Springfield, Virginia 22161

NASA-Langley, 1981